

RESEARCH

Open Access

Impulsive interference in communication channels and its mitigation by SPART and other nonlinear filters

Alexei V Nikitin^{1,2*}, Marc Epard², John B Lancaster^{1,2}, Robert L Lutes² and Eric A Shumaker²

Abstract

A strong digital communication transmitter in close physical proximity to a receiver of a weak signal can noticeably interfere with the latter even when the respective channels are tens or hundreds of megahertz apart. When time domain observations are made in the signal chain of the receiver between the first mixer and the baseband, this interference is likely to appear impulsive. The impulsive nature of this interference provides an opportunity to reduce its power by nonlinear filtering, improving the quality of the receiver channel. This article describes the mitigation, by a particular nonlinear filter, of the impulsive out-of-band (OOB) interference induced in High Speed Downlink Packet Access (HSDPA) by WiFi transmissions, protocols which coexist in many 3G smartphones and mobile hotspots. Our measurements show a decrease in the maximum error-free bit rate of a 1.95 GHz HSDPA receiver caused by the impulsive interference from an OOB 2.4 GHz WiFi transmission, sometimes down to a small fraction of the rate observed in the absence of the interference. We apply a nonlinear SPART filter to recover a noticeable portion of the lost rate and maintain an error-free connection under much higher levels of the WiFi interference than a receiver that does not contain such a filter. These measurements support our wider investigation of OOB interference resulting from digital modulation, which appears impulsive in a receiver, and its mitigation by nonlinear filters.

Keywords: electromagnetic interference, impulsive noise, interchannel interference, nonlinear filtering, out-of-band interference, SPART filter

1 Introduction and motivation

It is becoming more and more common that multiple digital communication devices coexist and concurrently operate in close physical proximity. A typical example would be a smartphone equipped with WiFi, Bluetooth, and GPS, and capable to operate at various data protocols and in multiple frequency bands. This physical proximity, combined with a wide range of possible transmit and receive powers, creates a variety of challenging interference scenarios. Plenty of empirical evidence indicates that such interference often manifests itself as impulsive noise [1,2], which in some instances dominates over the thermal noise [1,3].

A particular source of impulsive noise in digital communication systems is interchannel interference [4,5].

For example, a strong close transmitter (say, WiFi) can noticeably interfere with a receiver of a weak signal (say, GPS) even when the separation of their frequency bands exceeds the respective nominal bandwidths of the channels by orders of magnitude. When time domain observations of such far-OOB interference are made at the receiver frequency, in a relatively wide bandwidth to avoid excessive broadening of the transients, this interference is likely to appear impulsive. Understanding the mechanism of this interference and its impulsive nature is important for its effective mitigation.

As shown in [4,5], the fundamental origin of the interchannel interference lies in the unavoidable non-smoothness in the modulation of the interfering transmitter, which leads to discontinuities in the higher order derivatives of the modulating signal. This non-smoothness is exacerbated by the non-idealities in the hardware

* Correspondence: avn@avatekh.com

¹Avatekh Inc., 900 Massachusetts Street, Suite 409, Lawrence, KS 66044, USA
Full list of author information is available at the end of the article

implementation, and by the coupling of other interfering signals from the adjacent circuitry.

As outlined in [4-7], certain analog nonlinear filters deployed early in the signal chain of the receiver can improve the signal-to-noise ratio (SNR) and increase the data rates of a communication channel (e.g., GPS or WCDMA) in the presence of impulsive interchannel interference, for example, from WiFi transmissions. Although *analog* by definition, these filters can also be implemented digitally, for example, in FPGA or software, and, unlike other typical nonlinear filters such as median filters, they require little memory and computational resources and can operate in real time even at very high sampling rates.

In this article we present the measurements, under various experimental conditions, of the impact of a 2.412 GHz 802.11g (Channel 1) WiFi transmitter on the HSDPA protocol [8] running at 1.95 GHz in the UMTS-FDD band II downlink (used in the United States by AT&T Mobility), and quantify the improvement in the channel quality provided by a particular nonlinear filter, ‘SPART’, described in [6].^a This continues our wider investigation into the impulsive nature of the OOB interference from different digital modulation protocols, and the mitigation of impulsive noise by nonlinear filters.

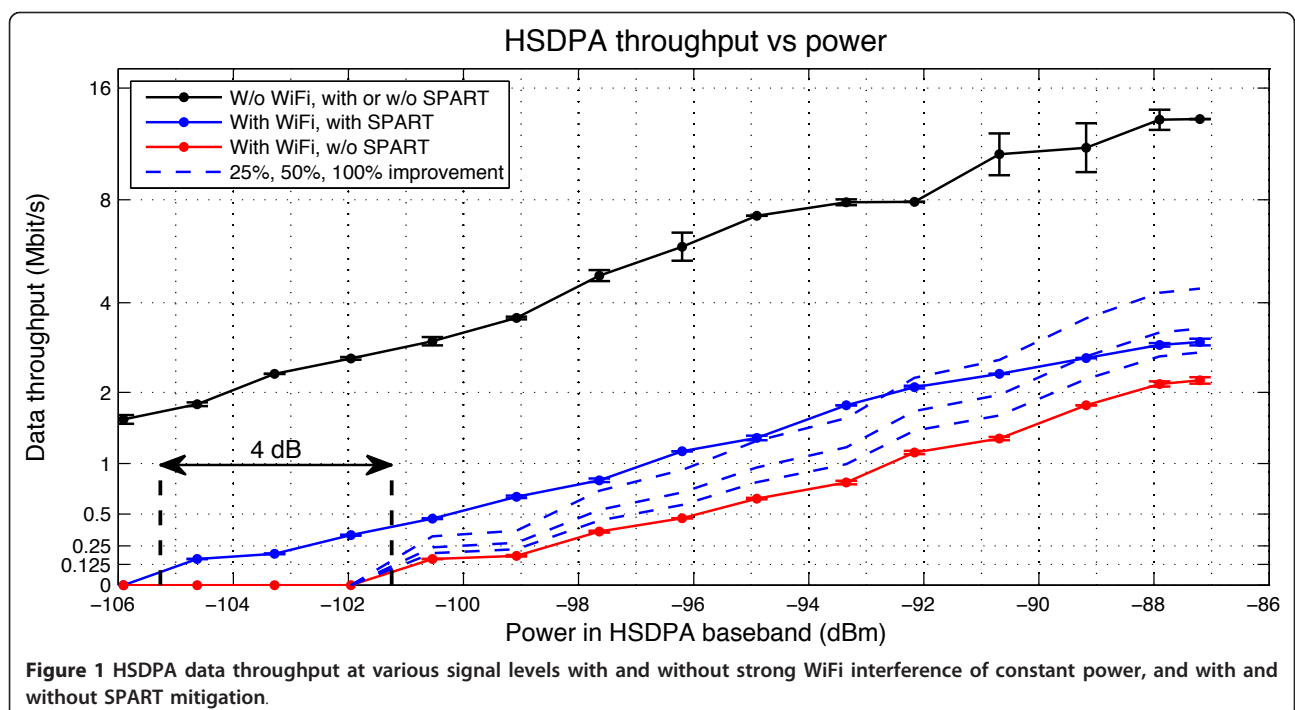
1.1 Main result

The main experimental result of this study is summarized in Figure 1. The figure shows the data throughput

of HSDPA at various signal levels with and without strong WiFi interference of constant power, and with and without the SPART filter deployed in the receiver signal chain.

In the figure, the black line shows the HSDPA throughput without the WiFi interference, and the insertion of the SPART filter in the signal chain of the receiver does not affect the data throughput. WiFi interference lowers the throughput and/or causes the loss of connection (red line). A SPART filter in the signal chain of the receiver recovers a portion of the lost data rate, and/or restores the lost connection (solid blue line). The error bars indicate the standard error of the measurements. For reference, dashed blue lines indicate 25, 50, and 100% improvement in the data rate, respectively. One can see that, when the SPART filter is used during the WiFi interference, the connection (positive throughput) is maintained for lower HSDPA signal levels. This effectively increases the link budget, as indicated by the horizontal black arrow line in the figure.

The result presented in Figure 1 supports the following two statements: (i) a strong WiFi transmitter can noticeably interfere with an HSDPA receiver even though their operating bands are almost half a GHz apart, and (ii) because of the impulsive nature of this interference, it can be mitigated by nonlinear filters such as, for example, the SPART filter used in this study. A detailed description and examples of the performance of other analog nonlinear filters for impulsive noise mitigation can be found in [5,7].



2 Test setup and procedures

The novel nonlinear nature of the proposed methodology for impulsive noise mitigation necessitates the introduction of a variety of rather atypical experimental considerations. These include the bandwidth along the signal processing chain, the filter placement, and the time domain characterization of the signal at different points. Also, as discussed in [4,5], the impulsive interference is exacerbated by the non-idealities in the hardware implementation, and thus is specific to the hardware. To adequately address these considerations and to ensure objective evaluation and reproducibility of our results, we provide a detailed description of the experimental setup and procedures. To improve the readability of the article, here we present an outline of the test setup and procedures, while relegating most of the details to the appendices.

2.1 System model

The experiment reported in this article models the effect of the OOB WiFi interference with an HSDPA channel, and its mitigation by SPART filters. The block diagram of the experimental setup is shown in Figure 2. The system models an HSDPA receiver and a WiFi transmitter operating concurrently in close physical proximity, which represents configurations found in many smartphone handsets as well as in mobile WiFi hotspots. The HSDPA signal level is relatively low (for example, due to being indoors and/or far away from the transmitter), while the WiFi signal level is relatively high. The connectors, cables, and attenuators in the respective signal chains before the bandstop filter in Figure 2 represent all respective losses at 1.95 GHz (measured approximately 83 dB total for the HSDPA, and 15 dB total for the WiFi), and are within the ranges encountered in real-life configurations.^b To further limit the coupling of the *in-band* WiFi signal into the HSDPA receiver channel, a bandstop filter is cascaded with an HSDPA preselect filter.

2.2 Hardware overview

For an HSDPA receiver, we used the Ettus Research software-defined radio (SDR) USRP N210 [9] with the DBSRX2 daughterboard [10]. The N210 board uses 100 MS/s analog-to-digital converters (ADCs), which allows signal processing in a relatively wide bandwidth before the baseband. The importance of high-rate sampling for this study is clarified later in the article. A manufactured cellular phone would not be appropriate for this study since the higher bandwidth nodes are inaccessible as they are internal to the receiver integrated circuit (IC). We used USRP2 SDR transmitters, one with the WBX daughterboard [10] for the HSDPA signal, and one with the XCVR2450 [10] for the WiFi.

For greater control and repeatability, instead of wireless connections, semi-rigid coaxial cables, attenuators, and a splitter/combiner were used for mixing the HSDPA and the WiFi signals. We used a shielded enclosure for the receiver to reduce unwanted signal coupling, and to avoid additional outside interference. A surface acoustic wave (SAW) preselect filter was connected to the antenna port of the receiver, and a bandstop filter, similar to those used in mobile WiFi hotspots, was added to further limit the coupling of the in-band WiFi signal into the HSDPA receiver channel. A computer connected to all three SDRs via gigabit Ethernet performed all control functions for the test procedures, implementation of the modulation protocols, and acquisition and analysis of data. More detail on the hardware setup and components can be found in Appendix 1.

2.3 Software-defined radios

The SDRs from Ettus Research implement the HSDPA and WiFi standards in MATLAB, including matched filtering, Code Division Multiple Access (CDMA) spreading/de-spreading, modulation/demodulation, forward error correction, bit error tests, etc., and to perform comprehensive analysis of the data using MATLAB

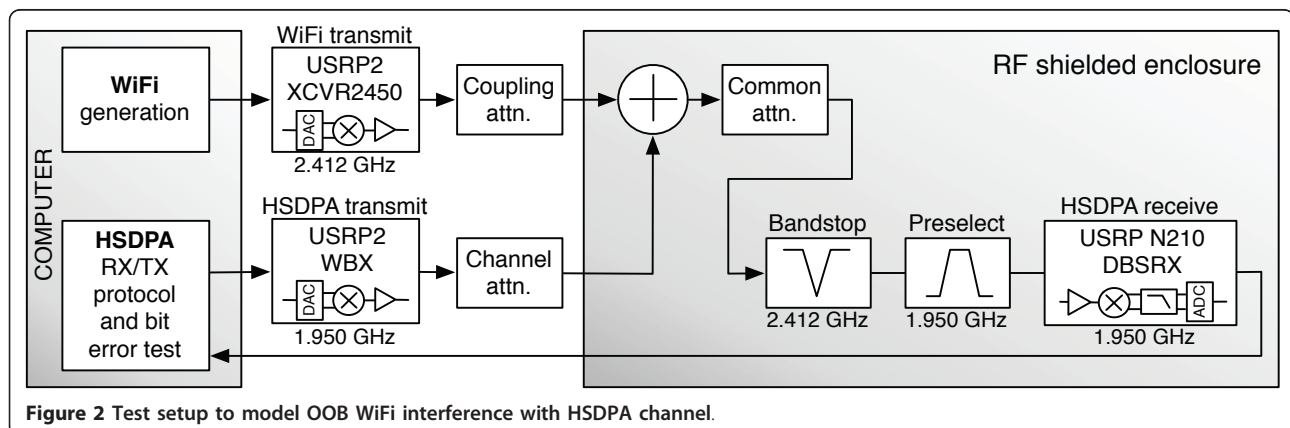


Figure 2 Test setup to model OOB WiFi interference with HSDPA channel.

software. A single computer coordinated all three SDRs, providing full control over the transmission, reception, data acquisition, and the signal processing functions. The field programmable gate array (FPGA) following the N210's 100 MS/s ADCs provides adequate flexibility and capacity to deploy and test a Verilog hardware description language (HDL) SPART filter implementation, though the results reported in this article were obtained with a MATLAB software SPART implementation. This simplified the development and provided the ability to process exactly the same received data with or without SPART.

Although the ADCs in the N210 board sample the incoming complex I/Q signal at 100 MS/s, the N210 decimates this to at most 25 MS/s, the maximum that can be streamed continuously over the Ethernet to the host computer. For our testing, we modified the firmware and implemented a procedure for capturing arbitrarily long files of received samples at the full 100 MS/s rate.

The host computer loads the signal blocks for transmission into random-access memory (RAM), and then simultaneously sends them to the appropriate SDRs. The receiver acquires the samples at the full 100 MS/s rate, saves them in the N210's high speed static random-access memory (SRAM), and sends them over the Ethernet to the host computer at lower rates. Since the N210s allow scheduling of transmits and receives with a precision of one tick of the 100 MHz ADC clock (10 ns), we schedule the transmission in a manner allowing us to construct a contiguous set of samples of the desired length, emulating a continuous real-time operation. This procedure is performed by a native C++ application using Ettus' Universal Hardware Driver (UHD) library [11].

For analysis, the MATLAB software reads the samples received by the N210, applies notch filters to remove harmonics of the clock signal that may appear in the DBSRX2 receiver board at high gains, optionally applies a SPART filter, and uses polyphase resampling to two complex samples per chip. It then applies the matched root raised cosine (RRC) filter, removes the padding and signal chain delay, corrects phase errors, de-channelizes, demodulates, performs rate de-matching, and applies forward error correction. By comparing the resulting bits with the transmitted pseudorandom bits, the software performs the bit error tests. The software can also conduct various time and frequency domain measurements at each processing stage.

2.4 SPART filter

The SPART filter used in this study is a complex-valued modification of the filter described in [6], where it was referred to as 'FrankenSPART'. This filter can be viewed

as an analog feedback circuit characterized by a *time constant* and a *rate* parameter, and having the following behavior: When the absolute value of the difference between the input and the output signals is small in comparison with the product of the time constant and the rate parameter, the absolute value of the rate of change of the output of the SPART circuit equals that of a 1st order (one-pole) lowpass filter having the same time constant. Otherwise, the absolute value of the rate of the output equals to the rate parameter. If a SPART circuit with sufficiently small time constant is deployed early in the signal chain of a receiver channel affected by non-Gaussian impulsive noise, it can be shown that there exists such rate parameter that maximizes SNR and improves the quality of the channel.

The response of a SPART filter approaches that of a 1st order lowpass filter with the same time constant in the limit of a large rate parameter, and thus, provided that the time constant is sufficiently small and that the rate parameter is sufficiently large, SPART never degrades the channel, regardless the noise composition.

Even though SPART is an *analog* filter, it can be easily implemented digitally, for example, in FPGA or software. A digital SPART requires very little memory and typically is computationally inexpensive, which makes it suitable for real-time implementations.

Mathematical description and an example of digital implementation of the complex-valued SPART filter used in this study are given in Appendix 2.

2.4.1 Filter placement

Since SPART is a *nonlinear* filter, its placement in the signal chain affects the outcome. For effective suppression of impulsive noise, a SPART filter should be deployed relatively early in the signal chain of the receiver. As discussed in [4,5], since the apparent peakedness for a given transmitter depends on the characteristics of the receiver, in particular its bandwidth, an effective approach to mitigating the OOB interference should be as follows: (i) allow the initial stage of the receiver to have a relatively large bandwidth so that the transients are not excessively broadened and the OOB interference remains highly impulsive, then (ii) implement the final reduction of the bandwidth to within the baseband specifications through nonlinear means, such as the analog filters described in [5-7,12-15].

In our experiment, the best placement option would be an analog SPART preceding the antialiasing filter, as shown in Figure 3a. However, this node is inaccessible as it is internal to an IC in the receiver.

Thus we used the option shown in Figure 3b, that is, a digital SPART at 100 MS/s. This placement, while adequate for the main purpose of the experiment reported in this article, would not be an optimal engineering choice. The major reason is that, in order to maintain a large

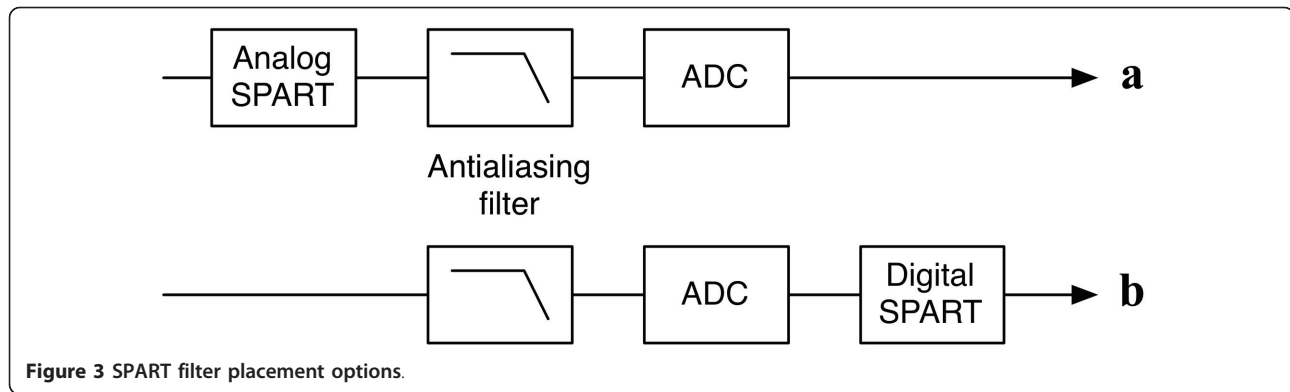


Figure 3 SPART filter placement options.

enough bandwidth for the SPART filter to be effective, the bandwidth of the antialiasing filter must be as large as possible. In the presence of sufficiently strong impulsive interference, however, large-bandwidth outliers are likely to be out of the ADC range. In order to prevent the ADC from saturating, the bandwidth of the antialiasing filter must be reduced, which decreases the effectiveness of the SPART filter. The effect of the antialiasing bandwidth on the SPART efficiency is discussed and illustrated further in the article. The ADC saturation issue is addressed in Section 4.1 and in Section “ADC saturation” in Appendix 3.

Even though the efficiency of a digital SPART is sub-optimal, digital and software implementations have advantages as they are easily modified and compared, and a SPART filter implemented in MATLAB behaves exactly as one implemented in an FPGA.

2.5 HSDPA protocol

High Speed Downlink Packet Access [8] carries data from the cellular base station to the user’s handset. Data bits are gathered into packets or frames of 2 ms, also known as the Transmission Time Interval (TTI). The base station encodes as many bits in a given frame as the signal conditions allow. The handset continuously evaluates the quality of the received signal and sends a Channel Quality Indicator (CQI) to the base station. The base station uses the CQI to determine how many bits to send in the next TTI allocated to that handset. The group of data bits encoded in each TTI is known as a Transport Block. It’s length is determined by the modulation, the number of CDMA channels used, and the forward error correction Code Rate. Better signal conditions allow more bits per symbol, more channels, and fewer bits devoted to error correction.

High Speed Downlink Packet Access is carried over wideband CDMA (WCDMA), which transmits 3,840,000 CDMA chips per second. Each HSDPA symbol is encoded using 16 chips (spreading factor 16), so each TTI contains 480 symbols ((TTI in seconds)×(chips per

second)/(chips per symbol)). HSDPA encodes 2 bits per symbol using QPSK (4-QAM) modulation, 4 bits per symbol using 16-QAM, or 6 bits per symbol using 64-QAM. Because each symbol is encoded in multiple chips, more than one stream, or channel, of symbols can be encoded in the same frame by using a different orthogonal channelization code for each channel. The spreading factor of 16 enables the use of 1 to 15 channels. Finally, HSDPA uses Turbo Coding [16] for forward error correction with an underlying code rate of 1/3, or 1 data bit for every three bits. By leaving out some of the data bits or error correction bits, known as puncturing, the effective code rate can be increased. Likewise, by repeating data or error correction bits, the effective code rate can be reduced. HSDPA uses puncturing or repetition in a process called ‘rate matching’, which matches the number of data bits and error correction bits (totaling three times the number of bits in the transport block) to the bits available in the TTI, which is determined by the bits per symbol, number of channels, and symbols per TTI.

Before the base station sends a transport block, it calculates and attaches a 24-bit cyclic redundancy code (CRC) to the user’s data. When the handset receives and decodes a transport block, it recalculates the block’s CRC and compares it with the one transmitted. If the CRC is not correct, the handset signals the base station, which triggers a retransmission in a future TTI. When retransmitting, the rate matching step may choose a different pattern of bits to puncture or repeat. When the handset receives the retransmission, it combines the bits it received previously with the new bits and reattempts error correction.

The mapping of the handset’s CQI to the number of bits encoded in each Transport Block is determined by tables associated with the handset’s User Equipment Category in the 3GPP standard. Our testing used 3GPP 25.214 Table 7G [[17], p. 61], with the exception of the first three entries, which our software does not support. The CQI values in our tests range from 1 to 27, which map to Transport Block sizes of 320 to 38,576 bits, for

through-puts of 160,000 to 19,288,000 bits per second, as shown in Figure 4, and in Table 1 in Section “CQI mapping table” of Appendix 4.

All HSDPA encoding and decoding was performed by MATLAB software developed by the authors, with some operations performed by the Coded Modulation Library (CML) version 1.0 [18]<http://www.iterativesolutions.com/Matlab.htm>.

For each CQI, our MATLAB software pre-computes sample data to be sent to the USRP2 for transmission by the WBX daughterboard. It generates pseudorandom bits for each transport block and encodes those bits using the modulation, number of channels and error correction for that CQI. It adds padding to the front and back of each group of frames to allow time for transmitters and receivers to settle and for delay through the transmit and receive signal processing chains. The software generates two complex I/Q samples per chip and applies RRC filtering as called for in the standard. It then uses polyphase resampling to up-sample to 25 million samples per second (MS/s), the maximum supported by the Ethernet connection to the USRP2, and saves the results to disk.

2.6 WiFi transmission

For WiFi, we use the FTW 802.11 package for GNU Radio [19]<https://www.cgran.org/wiki/ftw80211ofdm> to pre-compute standard 802.11g frames to be sent to a USRP2 for transmission by the XCVR2450 daughterboard. The FTW package uses Orthogonal Frequency Division Multiplexing (OFDM) and a user-specified data rate, modulation, and code rate, to encode data bits. It generates complex samples at 20 MS/s and saves them

on disk. We used 54 Mbit/s, 64-QAM and code rate 0.75 in our testing.

2.7 Test procedure

To evaluate the effect of the OOB WiFi interference, and quantify its mitigation by SPART filters, we asked the following question: “Given a set of signal and noise conditions, what is the maximum throughput that can be attained without bit errors and thus without retransmission?” Rather than emulating the handset’s quality measurements, we implemented a search procedure to determine the maximum throughput achievable. For each condition (signal transmitter power, WiFi presence or absence, SPART filter presence and settings), we conducted a binary search of the 27 CQI’s to find the maximum throughput that allowed ten successive Transport Blocks to be sent without any bit errors. We repeated the test forty times for each set of signal conditions, and results are presented as the mean of the forty tests with standard error bars.

We used the 1,950 MHz band for our HSDPA transmission, which is UARFCN channel 9750 in the UMTS-FDD operating band II downlink. We varied the HSDPA transmit power from -18 dBm to 2.6 dBm, the usable limits of the WBX transmitter, to create a range of signal strengths of -108 dBm to -87.4 dBm at the receiver input (after the bandstop and preselect filters). We transmitted WiFi at 2,412 MHz, which is 802.11g Channel 1, at a constant WiFi conducted power of 50 mW (17 dBm), which is significantly lower than the conducted power allowed and/or found in many 801.11g transmitters. For example, this is approximately five times (7 dB) lower than the 24 dBm

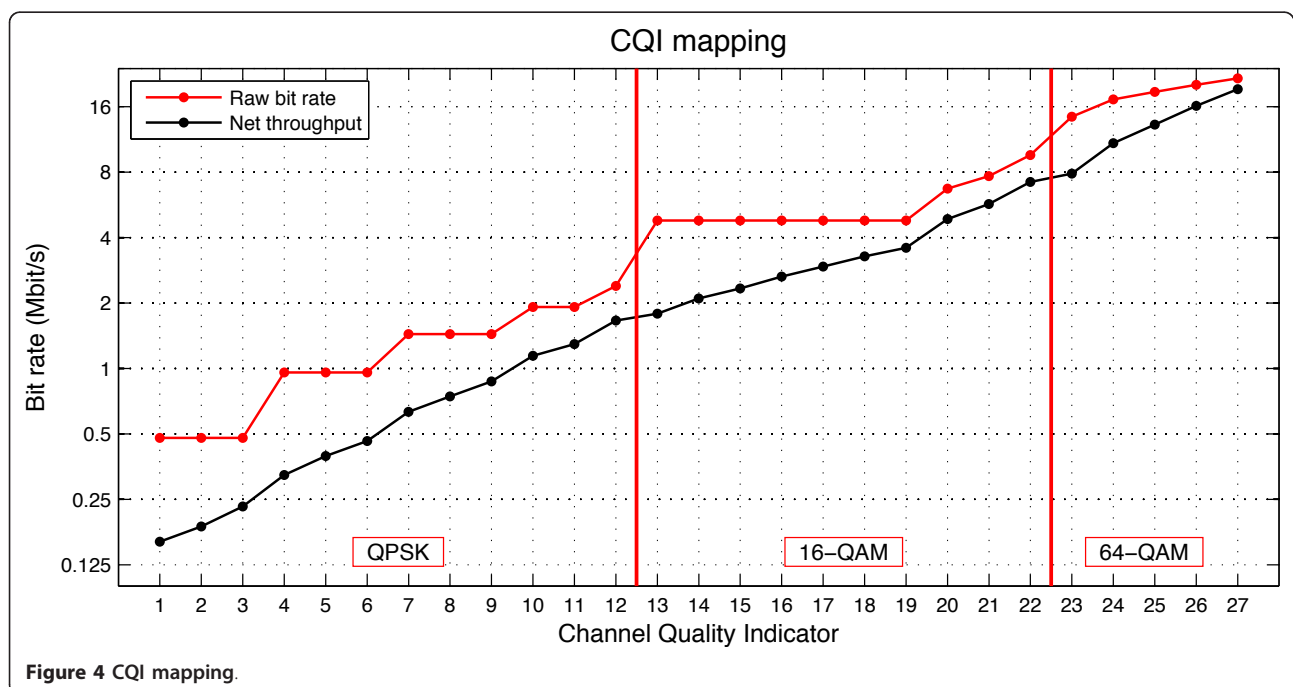


Figure 4 CQI mapping.

Table 1 CQI mapping table

| CQI from table 7G | HAI CQI mapping | Transport block size | Channels | Modulation | Bits per symbol | Total bits per TTI | Effective code rate | Throughput (bit/s) |
|-------------------|-----------------|----------------------|----------|------------|-----------------|--------------------|---------------------|--------------------|
| 1 | - | 136 | 1 | QPSK | 2 | 960 | 0.142 | 68,000 |
| 2 | - | 176 | 1 | QPSK | 2 | 960 | 0.183 | 88,000 |
| 3 | - | 232 | 1 | QPSK | 2 | 960 | 0.242 | 116,000 |
| 4 | 1 | 320 | 1 | QPSK | 2 | 960 | 0.333 | 160,000 |
| 5 | 2 | 376 | 1 | QPSK | 2 | 960 | 0.392 | 188,000 |
| 6 | 3 | 464 | 1 | QPSK | 2 | 960 | 0.483 | 232,000 |
| 7 | 4 | 648 | 2 | QPSK | 2 | 1,920 | 0.338 | 324,000 |
| 8 | 5 | 792 | 2 | QPSK | 2 | 1,920 | 0.413 | 396,000 |
| 9 | 6 | 928 | 2 | QPSK | 2 | 1,920 | 0.483 | 464,000 |
| 10 | 7 | 1,264 | 3 | QPSK | 2 | 2,880 | 0.439 | 632,000 |
| 11 | 8 | 1,488 | 3 | QPSK | 2 | 2,880 | 0.517 | 744,000 |
| 12 | 9 | 1,744 | 3 | QPSK | 2 | 2,880 | 0.606 | 872,000 |
| 13 | 10 | 2,288 | 4 | QPSK | 2 | 3,840 | 0.596 | 1,144,000 |
| 14 | 11 | 2,592 | 4 | QPSK | 2 | ,840 | 0.675 | 1,296,000 |
| 15 | 12 | 3,328 | 5 | QPSK | 2 | 4,800 | 0.693 | 1,664,000 |
| 16 | 13 | 3,576 | 5 | 16-QAM | 4 | 9,600 | 0.373 | 1,788,000 |
| 17 | 14 | 4,200 | 5 | 16-QAM | 4 | 9,600 | 0.438 | 2,100,000 |
| 18 | 15 | 4,672 | 5 | 16-QAM | 4 | 9,600 | 0.487 | 2,336,000 |
| 19 | 16 | 5,296 | 5 | 16-QAM | 4 | 9,600 | 0.552 | 2,648,000 |
| 20 | 17 | 5,896 | 5 | 16-QAM | 4 | 9,600 | 0.614 | 2,948,000 |
| 21 | 18 | 6,568 | 5 | 16-QAM | 4 | 9,600 | 0.684 | 3,284,000 |
| 22 | 19 | 7,184 | 5 | 16-QAM | 4 | 9,600 | 0.748 | 3,592,000 |
| 23 | 20 | 9,736 | 7 | 16-QAM | 4 | 13,440 | 0.724 | 4,868,000 |
| 24 | 21 | 11,432 | 8 | 16-QAM | 4 | 15,360 | 0.744 | 5,716,000 |
| 25 | 22 | 14,424 | 10 | 16-QAM | 4 | 19,200 | 0.751 | 7,212,000 |
| 26 | 23 | 15,776 | 10 | 64-QAM | 6 | 28,800 | 0.548 | 7,888,000 |
| 27 | 24 | 21,768 | 12 | 64-QAM | 6 | 34,560 | 0.630 | 10,884,000 |
| 28 | 25 | 26,504 | 13 | 64-QAM | 6 | 37,440 | 0.708 | 13,252,000 |
| 29 | 26 | 32,264 | 14 | 64-QAM | 6 | 40,320 | 0.800 | 16,132,000 |
| 30 | 27 | 38,576 | 15 | 64-QAM | 6 | 43,200 | 0.893 | 19,288,000 |

Summary listing of the modulation settings and associated bit rates for each CQI

WiFi conducted power at 2,412 MHz found in the Apple iPhone 4 [20].

We used a constant DBSRX2 gain setting of 65 dB, which combined with the 17.7 dB gain of the DBSRX2 low-noise amplifier (LNA) provides the total receiver gain of 82.7 dB.

3 Test results

This section is divided into two subsections. Section 3.1 focuses on the OOB WiFi interference, its impulsive nature, and the effect of the receiver bandwidth on the peakedness of this interference. Section 3.2 addresses the SPART performance and its effect on the data throughput.

3.1 OOB WiFi interference and its impulsive nature

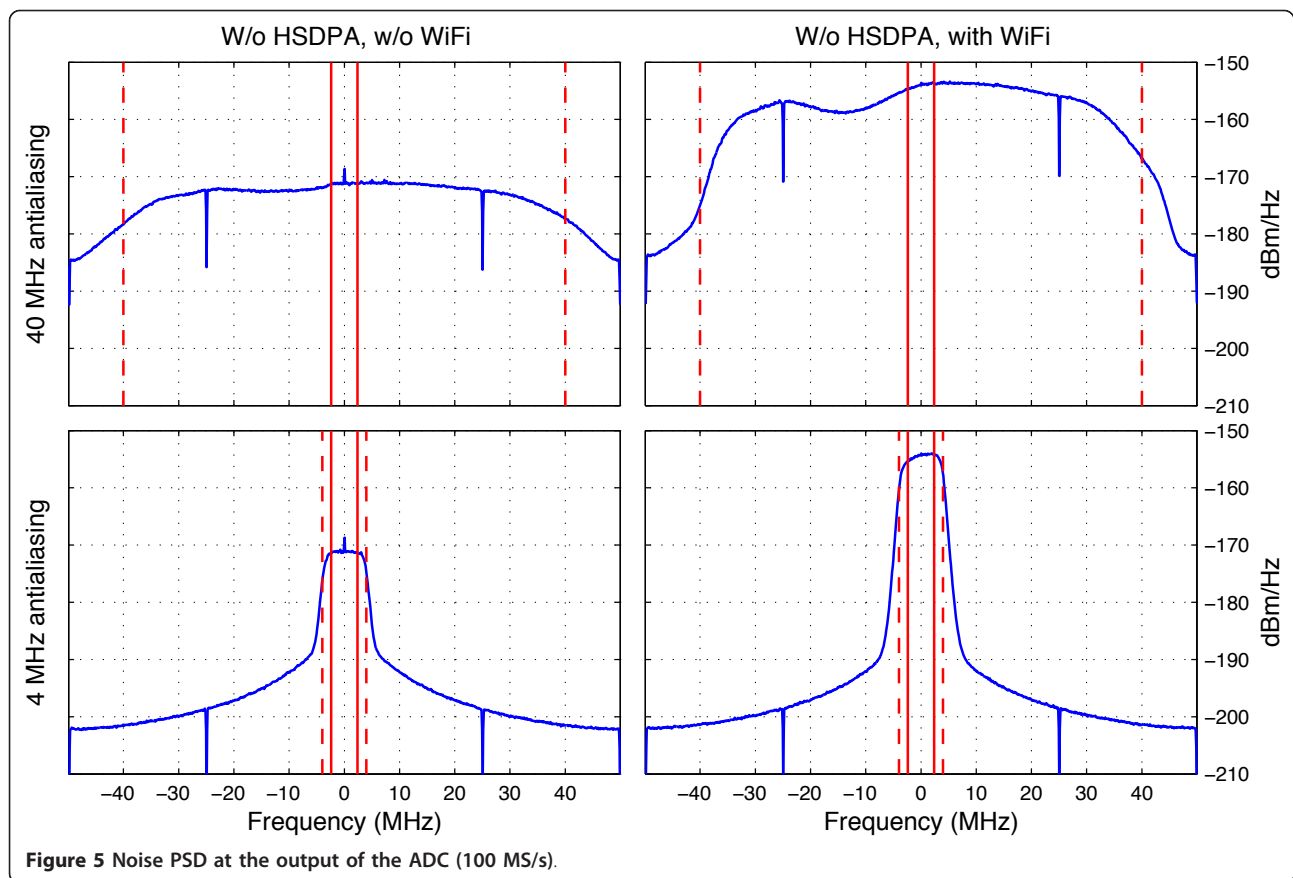
3.1.1 Noise power spectral density

Figure 5 shows the power spectral densities (PSD) of the HSDPA receiver noise at our fixed receiver gain of 82.7

dB, with and without WiFi interference. The spectra are computed as periodograms of the complex I/Q outputs of the 100 MS/s ADC signals, properly normalized to the dBm/Hz units based on the calibration measurements described in Appendix 3. The spectra are measured for two antialiasing bandwidths, wide (≈ 40 MHz) and narrow (≈ 4 MHz). The vertical dashed red lines indicate the nominal bandwidths of the antialiasing filters, and the baseband of the HSDPA signal is shown by the solid red lines. Figure 6 shows the same spectra as Figure 5, with different limits in the axes (zoomed-in).

The temperature during the measurements was maintained at approximately 302 K (84°F), leading to the -176.8 dBm/Hz expected value for the two-sided PSD of the thermal noise.

One can see that the measured receiver noise is approximately -171 dBm/Hz, which implies the noise figure for the receiver slightly under 6 dB. This is



consistent with the 5 dB noise figure reported by Ettus Research for the DBSRX2 daughterboard operating at the corresponding frequency and gain settings [10].

One can see from Figures 5 and 6 that the noise added by WiFi is approximately white within the anti-aliasing bandwidth, and that it contributes approximately 17 dB (50 times) to the rise in the total noise floor in the HSDPA baseband. The PSD, however, cannot reveal the impulsive nature of the OOB WiFi interference.

3.1.2 Time domain traces

The impulsiveness of the OOB WiFi interference becomes apparent when it is observed in the time domain. For example, Figure 7 shows the I/Q time domain traces of the noise measured at the outputs of the ADCs in the receiver. One can see, in the upper right panel of the figure, that the OOB WiFi interference added to the total receiver noise is visually impulsive when observed with a wide anti-aliasing bandwidth. One can also see that the reduction in the anti-aliasing bandwidth causes the impulsive transients to broaden, reducing the apparent impulsiveness of the noise (lower right panel).

3.1.3 Amplitude density and peakedness

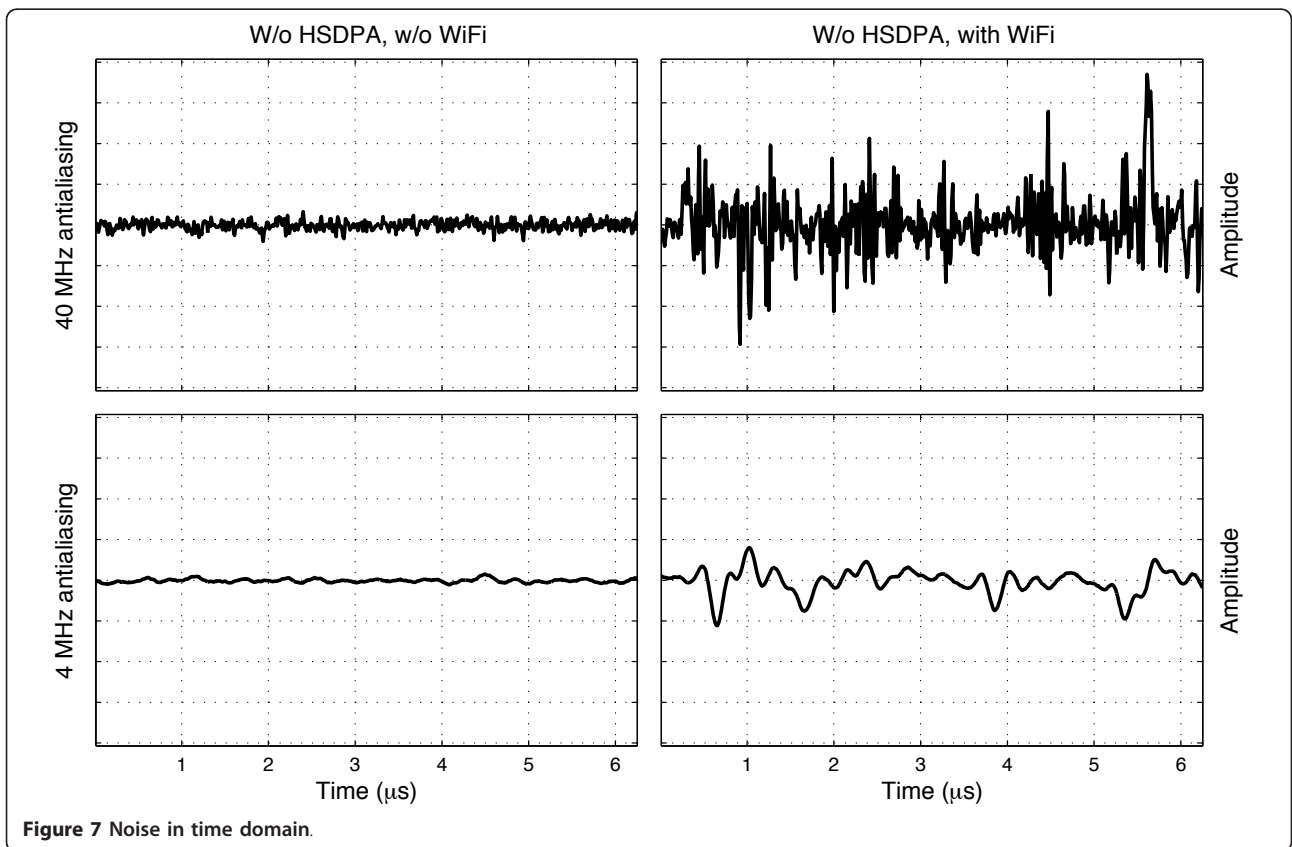
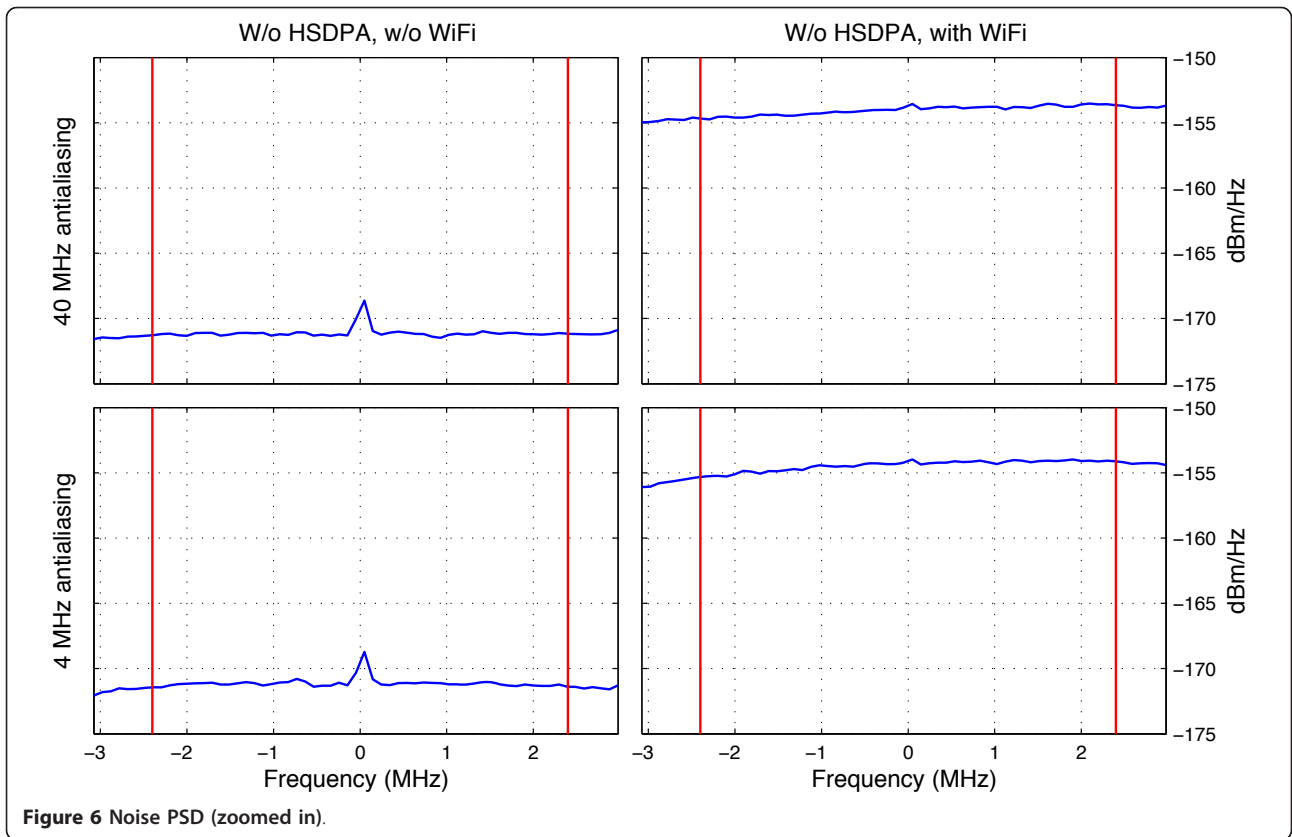
The impulsiveness of the noise can be quantified by its peakedness (measured in units “decibels relative to Gaussian” (dBG) [6]), defined in terms of *kurtosis* [21]

in relation to the kurtosis of the Gaussian (aka *normal*) distribution. By definition, the Gaussian distribution has zero dBG peakedness. Impulsive noise would thus have a higher peakedness than the Gaussian distribution (positive dBG). In time domain, high peakedness means a higher occurrence of outliers. In terms of the amplitude distribution of the signal, positive dBG peakedness translates into ‘heavier tails’ than those of the Gaussian distribution.

Figure 8 compares the amplitude densities and peakedness of the receiver noise of σ^2 total power with and without WiFi interference, and with wide and narrow anti-aliasing bandwidths. One can see that (i) the OOB WiFi interference increases the total peakedness of the noise, making it more impulsive, and that (ii) narrowing the bandwidth with linear filtering (anti-aliasing and/or baseband RRC) reduces peakedness, making the amplitude distribution of the noise approach Gaussian.

Figure 9 makes the ‘thickening of the tails’ of the noise distribution due to the OOB WiFi interference more apparent by showing the noise amplitude densities on a logarithmic scale. This thickening of the tails also manifests itself through the increase in peakedness.

In the upper left panel of Figure 9, at the limits of the amplitude range one can see peaks in the amplitude



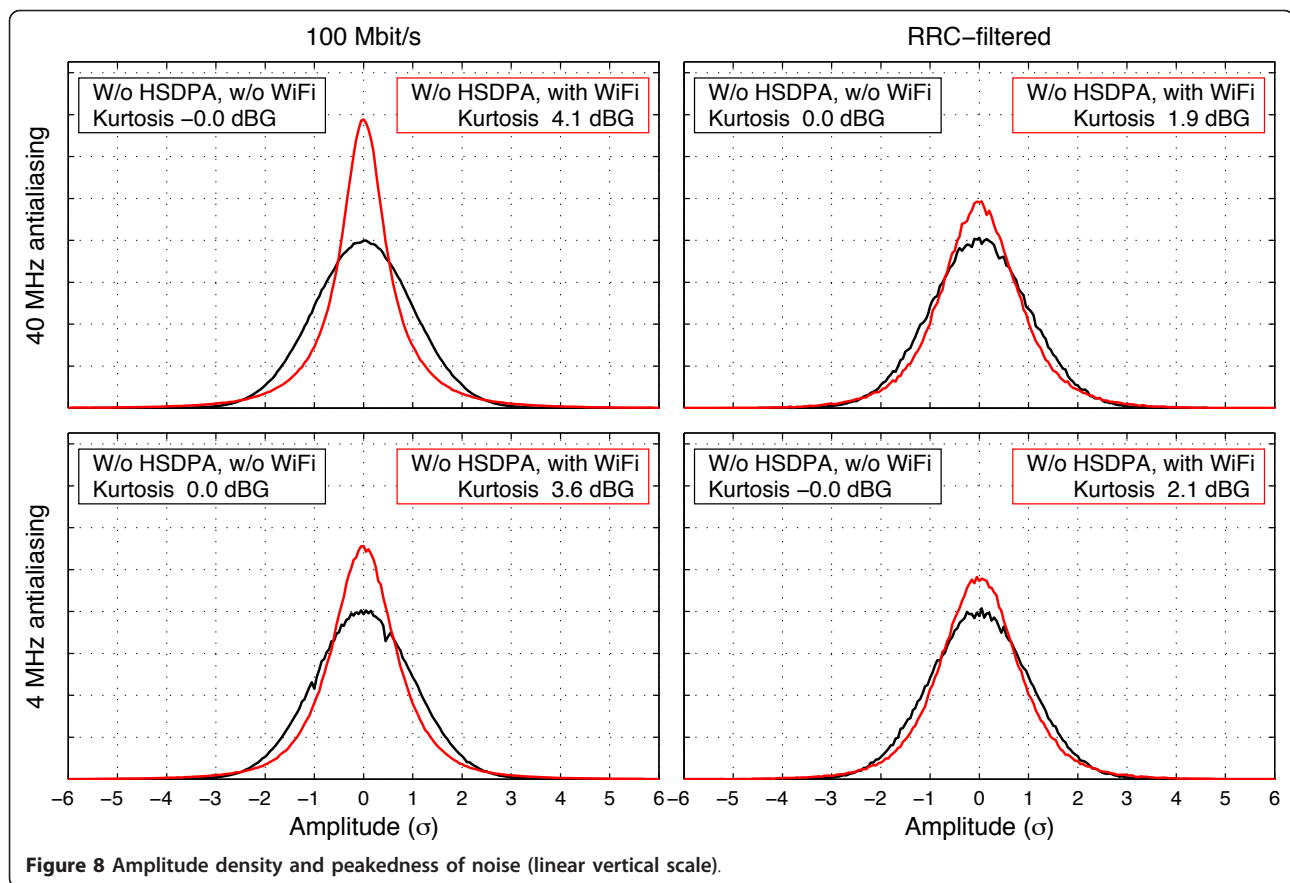


Figure 8 Amplitude density and peakedness of noise (linear vertical scale).

distribution of the noise with the OOB WiFi (red line). These peaks are indicative of the ADC saturation.^c

For SPART to be effective in suppression of the impulsive noise, the latter needs to be present to begin with. This is why a SPART filter needs to be deployed early enough in the signal chain, while the bandwidth is relatively large and the transients are not excessively broadened.

3.2 SPART effect on HSDPA throughput

The main test results are summarized in Figures 10 and 11. Both figures show the data throughput of HSDPA at various signal levels with and without strong WiFi interference of constant power, and with and without the SPART filter deployed in the receiver signal chain. In Figure 10, a wide bandwidth (40 MHz) ADC antialiasing filter was used. In Figure 11, a narrow bandwidth (4 MHz) antialiasing filter was used to illustrate the importance of the SPART placement at a wide bandwidth node in the signal chain.

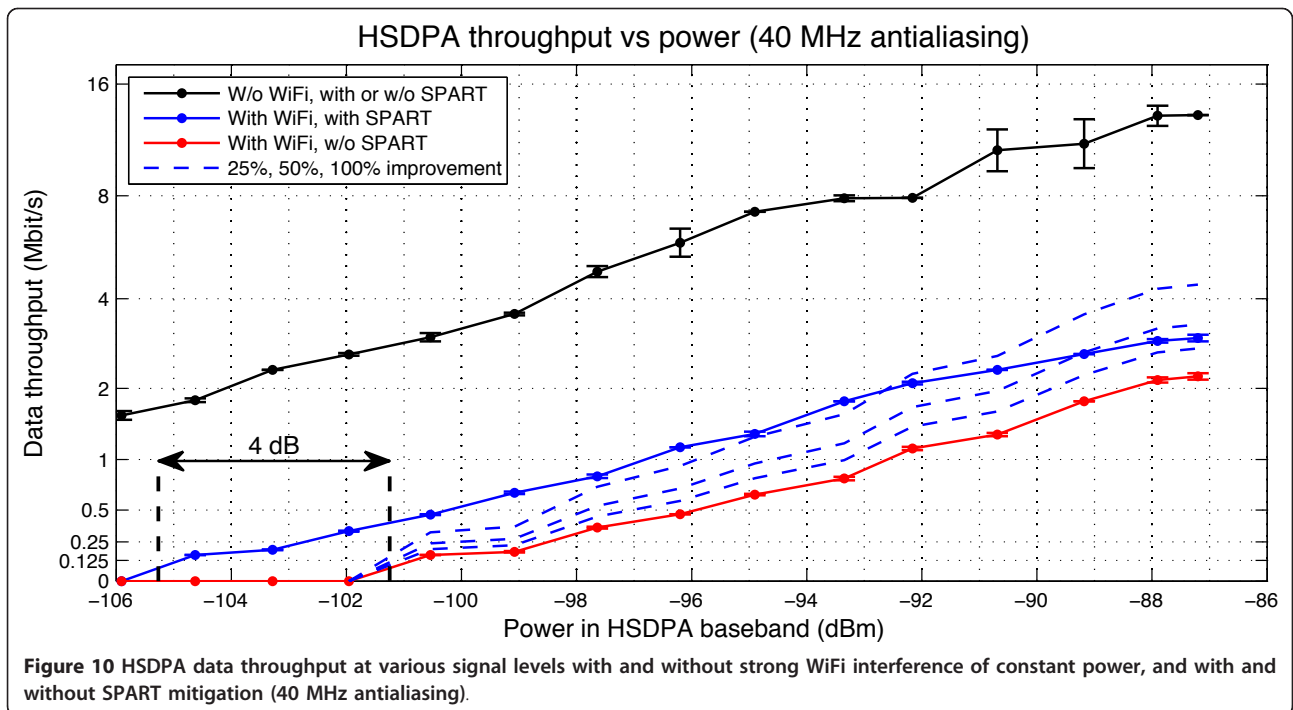
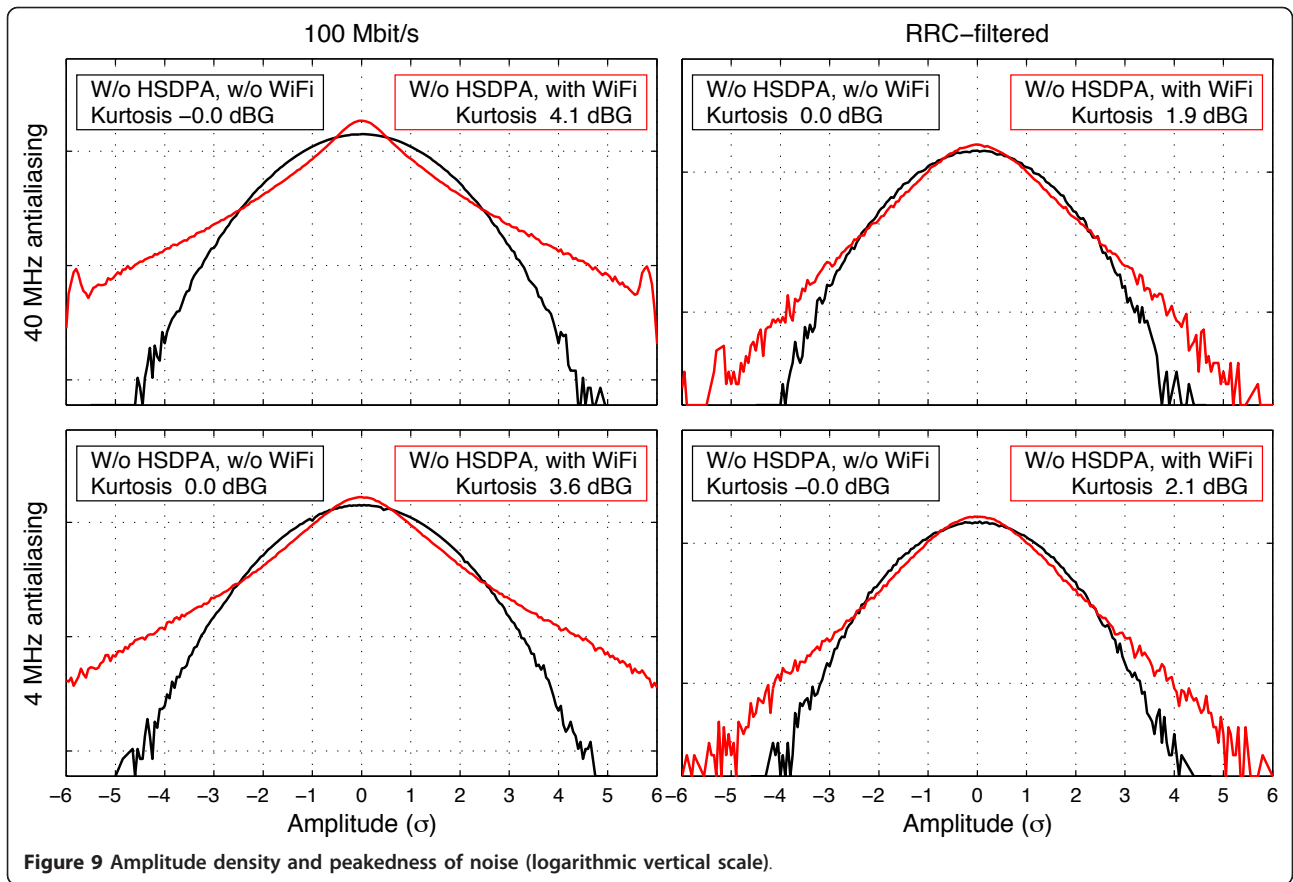
In both figures, the black lines show the HSDPA throughput without the WiFi interference, and the insertion of the SPART filter in the signal chain of the receiver does not affect the data throughput. WiFi interference

lowers the throughput and/or causes the loss of connection (red lines). A SPART filter in the signal chain of the receiver recovers a portion of the lost data rate, and/or restores the lost connection (solid blue lines). The error bars indicate the standard error of the measurements. For reference, dashed blue lines indicate 25, 50, and 100% improvement in the data rate, respectively.

One can see that, when the SPART filter is used during the WiFi interference, the connection (positive throughput) is maintained for lower HSDPA signal levels. This effectively increases the link budget, as indicated by the horizontal black arrow lines in both figures. By comparing Figures 10 and 11, one can also see that the SPART filter is much less effective when the narrow-bandwidth antialiasing is used.

3.2.1 Throughput recovery characterization

Figure 12 quantifies and compares the HSDPA throughput recovery achieved by the SPART filter, by showing the throughput improvement due to SPART as a percentage of the throughput without SPART, for both wide (blue line) and narrow (red line) antialiasing bandwidths. Similar to Figures 10 and 11, the increase in the link budget for both cases is shown by the horizontal black arrow lines.



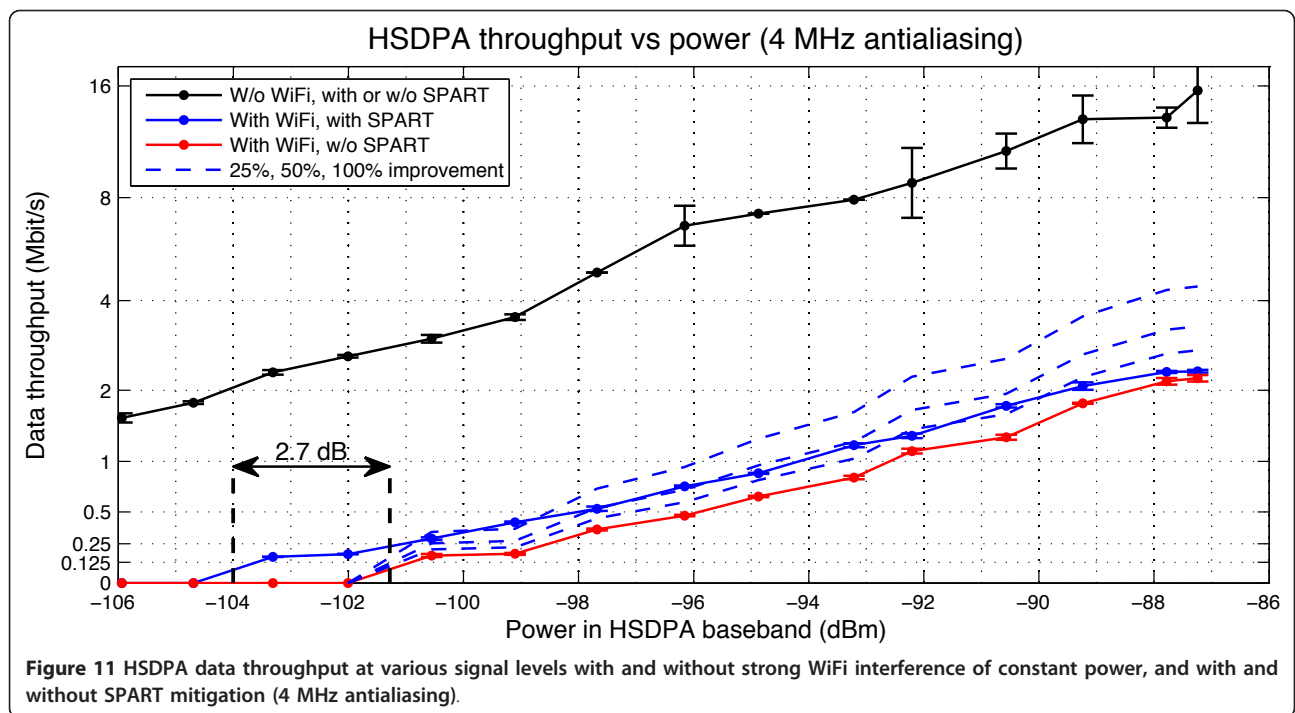
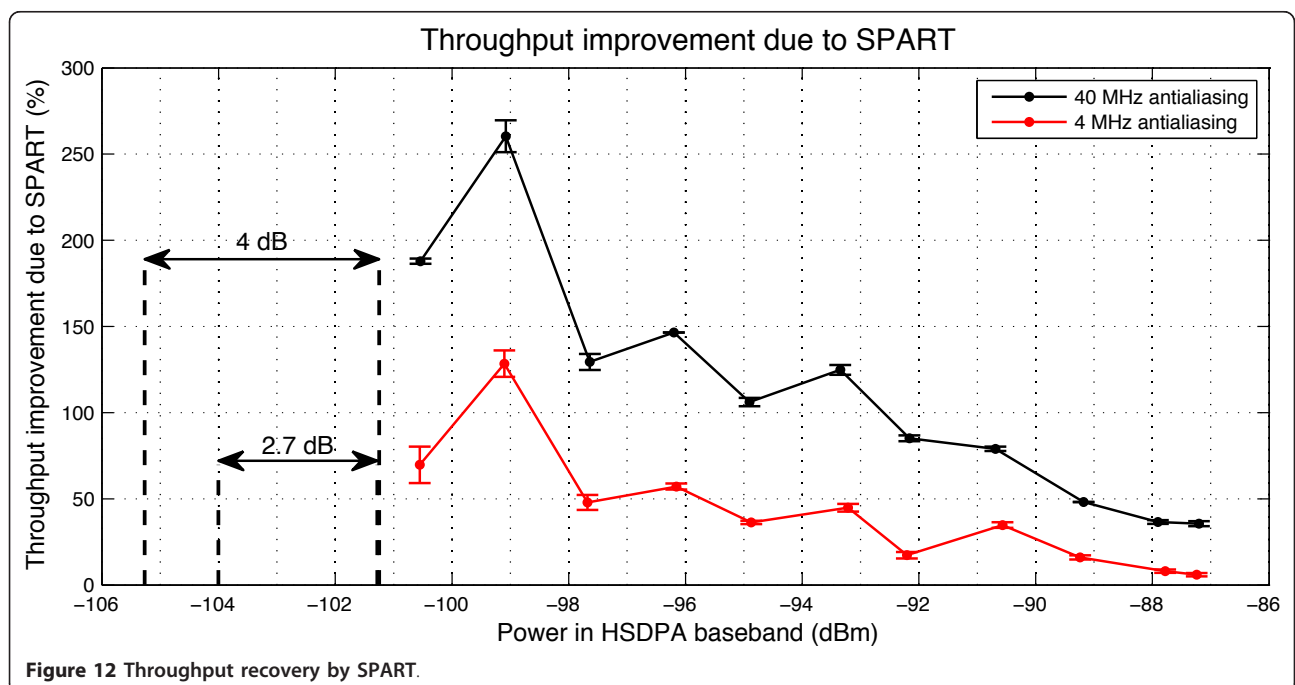


Figure 13 shows the effect of OOB WiFi on received signal bit error rate (BER) constellations, after forward error correction, when the measured HSDPA power is -101 dBm, and the CQI is 6 (QPSK modulation). Darker shading of the dots indicates higher likelihood of being correct, that is, lower BER. Again, one can see that the

SPART filter is more effective at wider antialiasing bandwidth.

3.2.2 Signal-to-noise ratios

Figures 14 and 15 show the SNRs for the HSDPA signal, measured at various signal levels with and without WiFi interference, and with and without the SPART filter. In



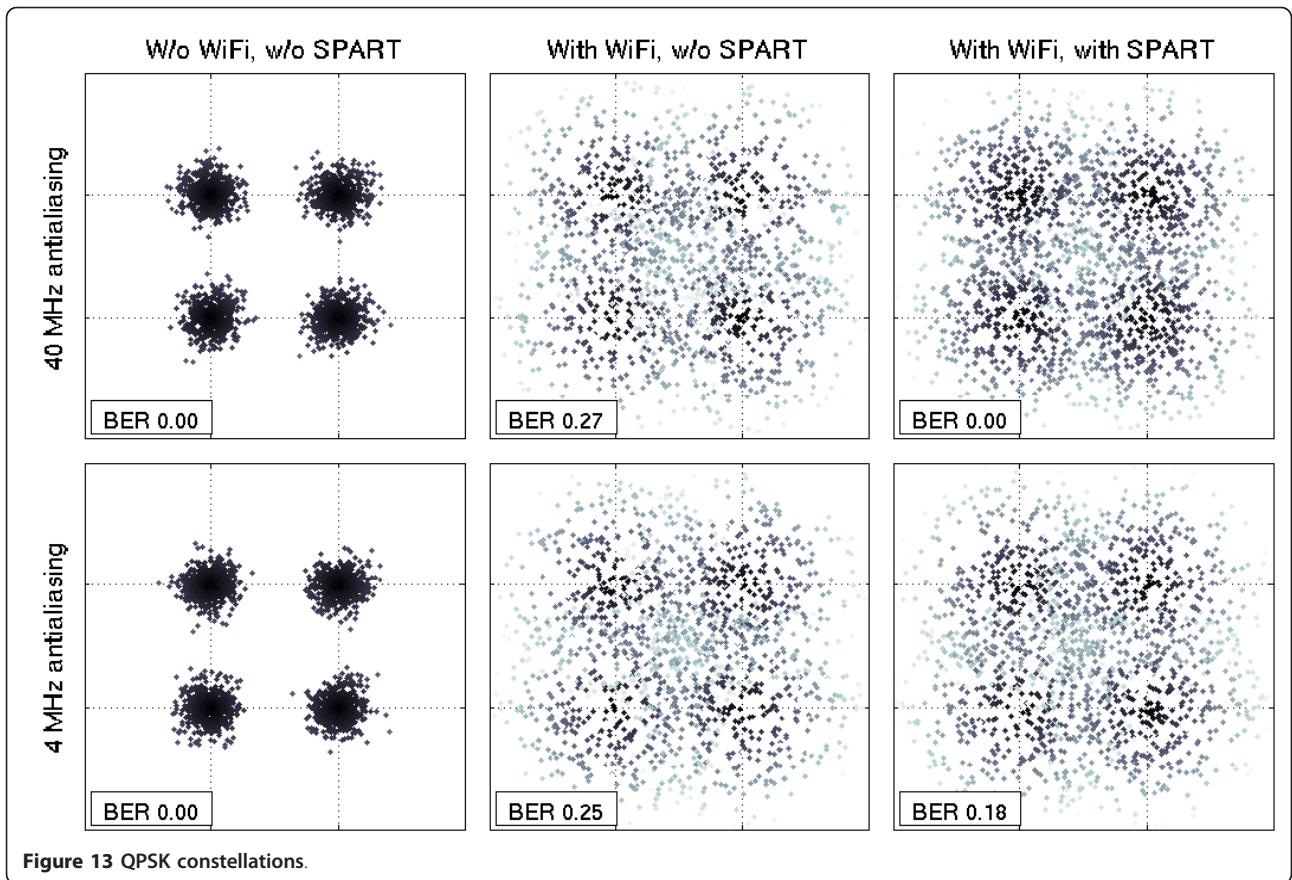


Figure 13 QPSK constellations.

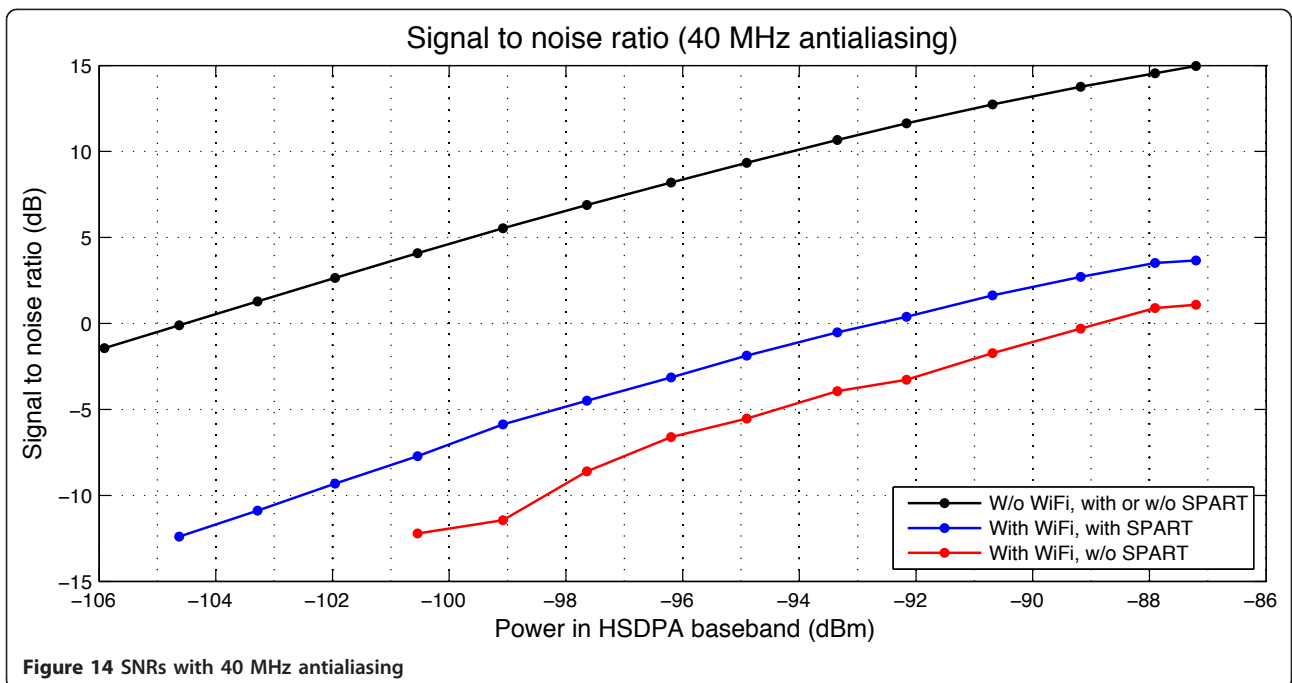


Figure 14 SNRs with 40 MHz antialiasing

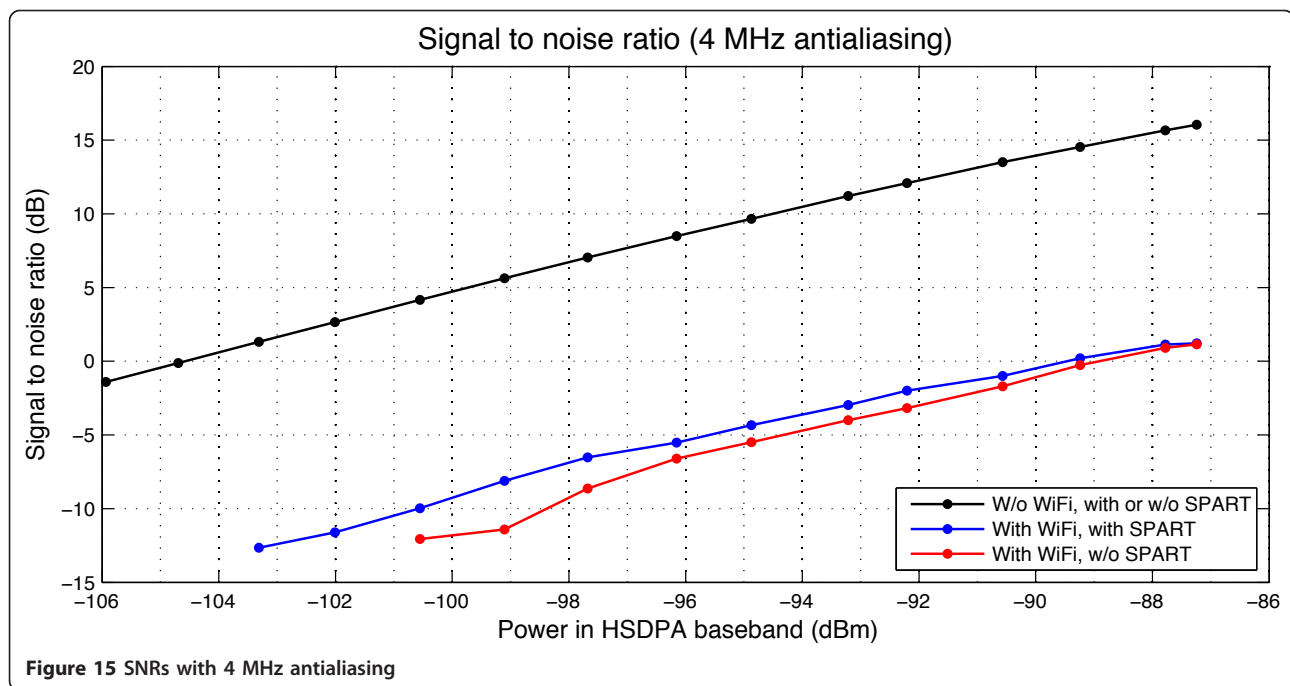


Figure 15 SNRs with 4 MHz antialiasing

Figure 14, the antialiasing bandwidth is 40 MHz, while in Figure 15 the antialiasing bandwidth is 4 MHz. The SPART filter, again, provides a greater improvement in the SNR when used at a higher bandwidth, before the outliers are excessively broadened.

3.2.3 Power spectral densities

Figure 16 shows the PSDs of the -89 dBm HSDPA signal with noise (with and without WiFi interference) at the output of the ADC at 100 MS/s. The vertical dashed red lines indicate the nominal bandwidths of the antialiasing filters, and the baseband of the HSDPA signal is shown by the solid red lines.

Figure 17 compares the PSDs at 100 MS/s (before decimation) for the cases with and without WiFi interference, and with and without SPART filter. The vertical red lines indicate the baseband of the HSDPA signal. One can see that, in the case of the 40 MHz antialiasing, the SPART filter lowers the noise floor by approximately a factor of two (3 dB).

Figure 18 compares the PSDs in baseband for the cases with and without WiFi interference, and with and without SPART filter. Blue lines show the PSDs of the HSDPA signal with noise, and the red lines show the PSDs of the extracted noise.

3.2.4 Time domain traces

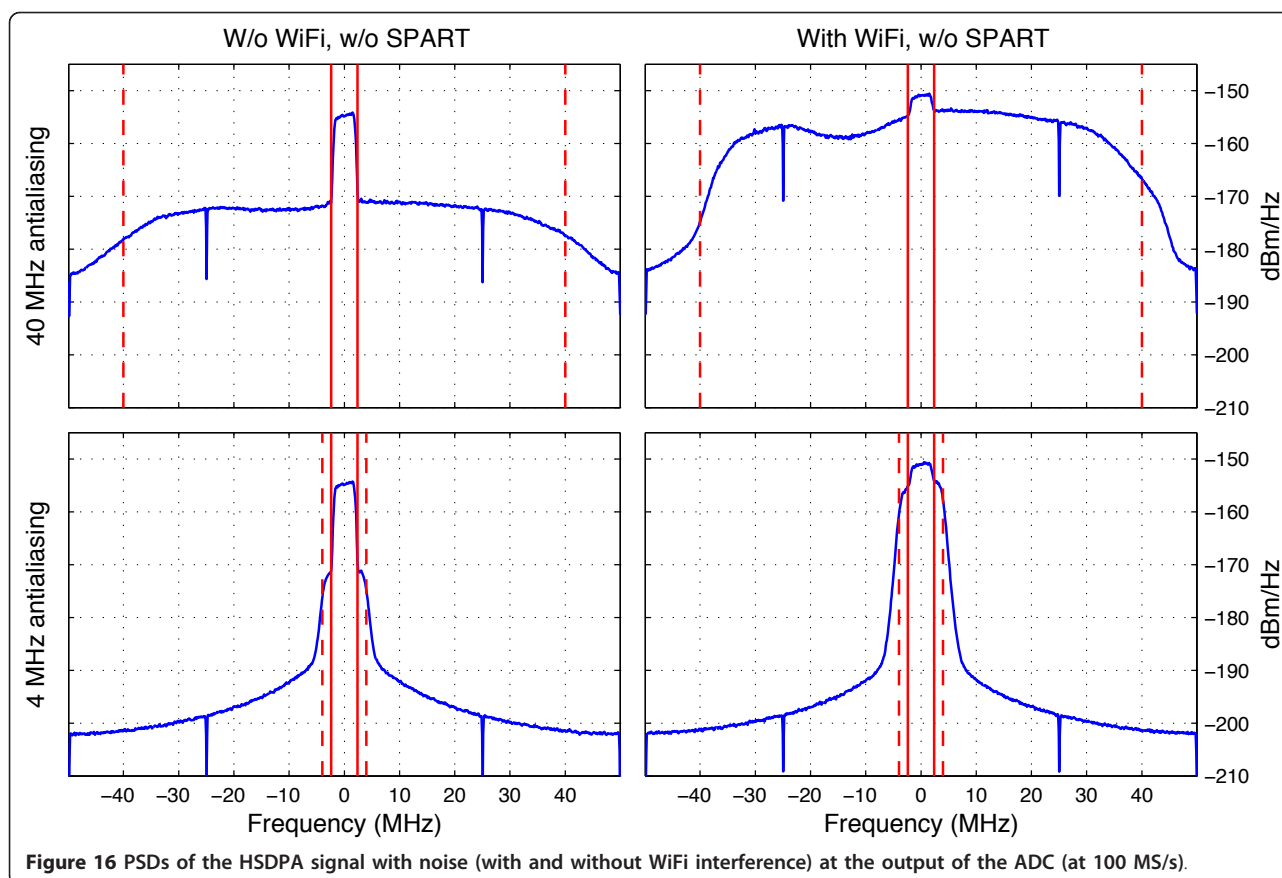
The time domain I/Q traces shown in Figure 19 provide another useful look at how the SPART trims the outliers while maintaining the signal of interest. In the figure, the ADC output sampled at 100 MS/s, with and without SPART, is shown by the blue lines, while the underlying HSDPA signal (CQI 15) is shown by the red lines. By

visual inspection of the deviation of the blue and red traces in the right-hand panels of the figure from each other, one can see that the OOB WiFi interference is more impulsive, and SPART is more effective, when a wider antialiasing bandwidth is used. After the signal shown by the blue traces is further filtered to within the baseband, this reduced deviation results in greater final improvement in the signal quality.

The time domain I/Q traces in Figure 20 show that the impulsive nature of the OOB WiFi interference becomes completely hidden as the bandwidth is reduced to within the HSDPA baseband, making the total noise appear Gaussian, and rendering the SPART filter ineffective if applied to the baseband signal.

3.2.5 Qualitative comparison with simulated examples

In order to clarify the mechanism of improving the signal quality by a SPART filter in the presence of impulsive noise, in Appendix 2 we provide simulated illustrations that can be used for qualitative comparison with the experimental results. In particular, Figure 21 shows the PSDs and the time domain traces of the input and the outputs of a SPART filter applied to a model signal + noise mixture with the characteristics (the noise bandwidth and kurtosis, and the SNR) comparable with those encountered in the experiment presented in this study. PSD shown in Figures 16 (the upper right panel) and 17 (the upper middle and the upper right panels) should be qualitatively compared with the PSDs shown in panels I, II, and III, respectively, of Figure 21. Likewise, the time domain traces shown in the upper middle and the upper right panels of Figure



19 should be qualitatively compared with the time domain traces shown in panels I and III, respectively, of Figure 21. The detailed description of Figure 21 is provided in Appendix 2.

4 Summary and discussion

The results presented in this article are a part of our wider investigation into the nature of the OOB interference from digital communications transmitters, which appears impulsive in a receiver, and its mitigation by nonlinear filters.

We have shown, through time domain measurements, that the noise introduced by an OOB WiFi interference in an HSDPA receiver is non-Gaussian and impulsive, and thus can be effectively mitigated by nonlinear means. We have observed and measured the decrease in maximum error-free bit rate of a 1.95 GHz HSDPA receiver caused by impulsive interference from an OOB 2.4 GHz WiFi transmission under certain experimental conditions, and quantified the throughput recovery enabled by a particular nonlinear filter, SPART, deployed early in the signal chain of the receiver.

Our measurements show that the error-free bit rate of HSDPA may significantly decline during the WiFi transmission, sometimes down to a small fraction of the rate

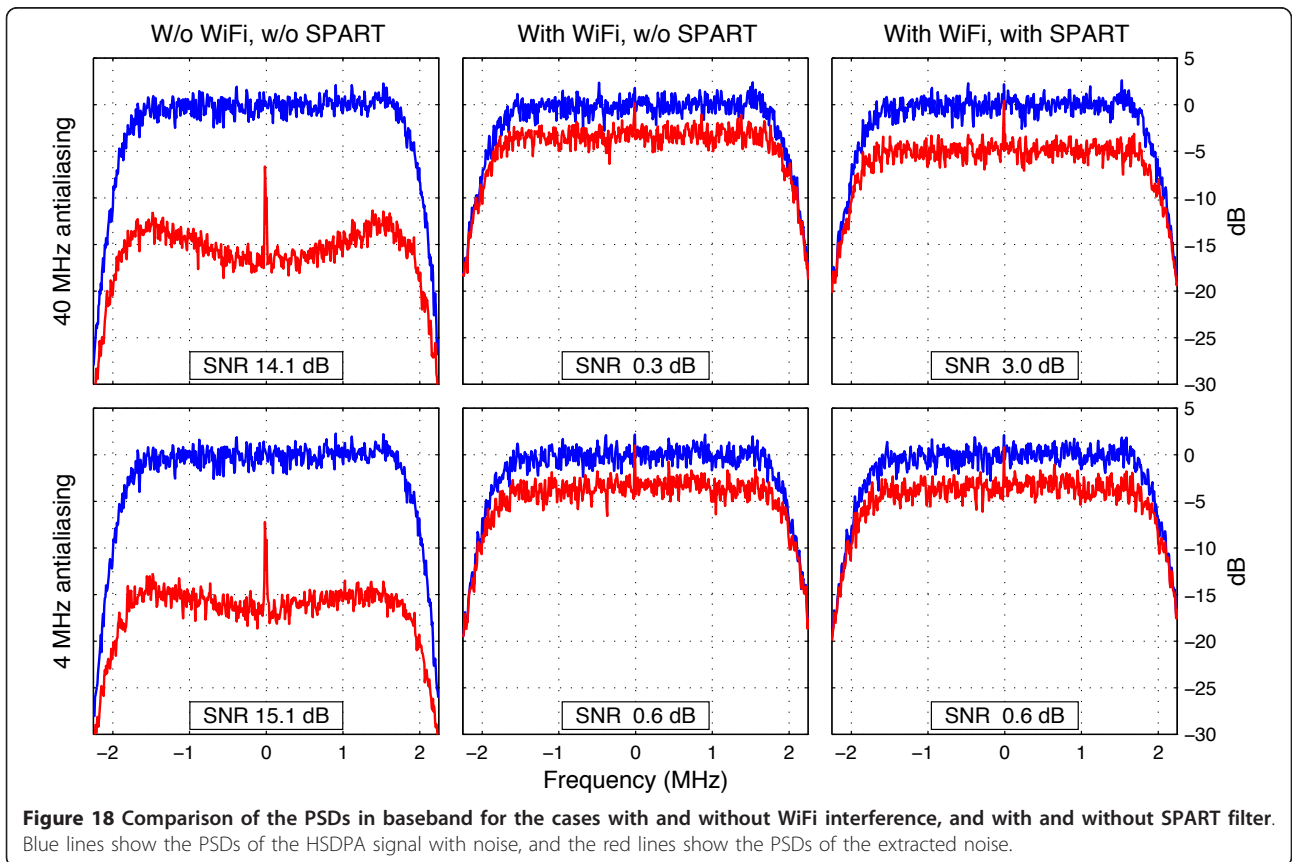
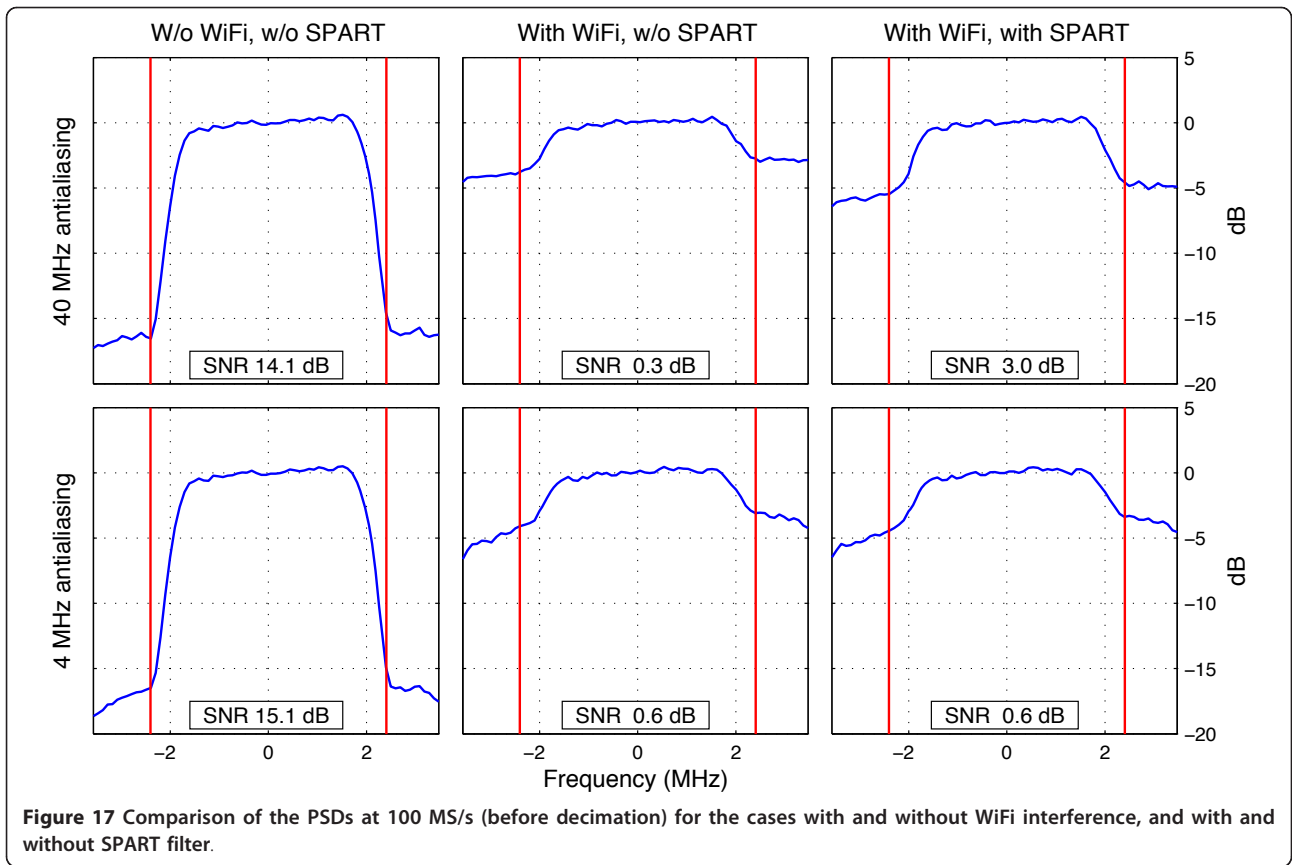
observed in the absence of the WiFi interference, which leads to an early loss of connection. A SPART filter inserted early in the signal processing chain of the receiver (before baseband) can recover a noticeable portion of the lost rate, and enables to maintain an error-free connection under much higher levels of the WiFi interference than a receiver that does not contain such a filter.

We have also discussed and demonstrated the importance of the appropriate filter placement in the signal chain, the associated bandwidth considerations, and the ‘analog vs. digital’ SPART implementations.

4.1 Constraints of the experiment

The experiment reported in this article is subject to the following constraints: (i) simplifications in the model, (ii) sub-optimal filter implementation and placement, and (iii) exclusion of the experimental results for the alternatives to the SPART filter.

The main constraint of our experiment is simplifications in the model. First, in order to achieve high reliability and reproducibility of our results, we used coaxial cables instead of wireless connections, and thus did not consider time-varying fading effects associated with wireless propagation. Also, we only tested the reception



of the HSDPA protocol of a single signal channel at 1.95 GHz in the UMTS-FDD band II downlink, and considered only one interference source (2.412 GHz Channel 1 of the 802.11g WiFi). Of course, a real world system would be affected by many more impulsive (and non-impulsive) interference sources. In order to keep our focus on the main goals of the presentation, we did not model and test a more realistic full system with multiple handsets, towers, and multiple signals, competing for bandwidth and time slots.

As discussed in Section 2.4.1, we used a sub-optimal SPART implementation (digital) and placement (after the ADC instead of prior to antialiasing), since the optimal analog location is internal to an IC in the receiver and thus inaccessible. To increase the effectiveness of SPART, we had to broaden the antialiasing bandwidth, which caused the ADC to saturate at high amplitude OOB WiFi outliers, diminishing filter performance. An analog SPART filter deployed prior to antialiasing would have been able to utilize the full bandwidth of the preselect filter, and would have prevented the ADC from saturating.

Further, our theoretical analysis and simulations show that several alternative nonlinear filters such as, for example, those described in [5,7] can provide better performance under the conditions of our experiment. However, the filter placement constraint discussed above undermines the usefulness of presenting the side-by-side comparison of the SPART filter with its alternatives in this study.

4.1.1 SPART effect on HSDPA throughput at lower WiFi power

Another limitation of the experiment is that we used a WiFi source of a constant, relatively high power. We used the WiFi conducted power of 50 mW (17 dBm), and assumed the -15 dB coupling between the HSDPA and WiFi antennas at the HSDPA signal frequency.

This is roughly equivalent, for example, to the iPhone 4 transmitting 2,412 MHz WiFi at 24 dBm [20], and having the antenna coupling of -22 dB at 1.95 GHz. While this appears feasible based on our bench measurements for small antennas separated by approximately 3.5 inches, and on the reported -13 to -30 dB mutual coupling between MIMO antennas of similar types and separation [22,23], we do not have solid experimental data to support this assumption for real life devices.

However, as follows from the above discussion, any reduction in antenna coupling resulting in a smaller impulsive noise contribution can be counteracted, in terms of the effectiveness of its mitigation, by (i) an appropriate filter placement, and (ii) by using more effective nonlinear filter alternatives. Even without these improvements, as illustrated in Figures 22 and 23, the setup used in this study can be used to demonstrate the

effectiveness of our approach at much lower OOB WiFi interference levels.

Figures 22 and 23 show the HSDPA data throughput at various signal levels for a 10 dB higher OOB WiFi path attenuation, which corresponds to over 30 dB coupling attenuation in the iPhone 4 example above. As can be seen in the figures, although the rise in the noise floor due to the impulsive OOB WiFi is now under 8 dB (as opposed to the 17 dB rise in the previous results; see Appendix 3 for details), the insertion of the SPART filter still provides a measurable throughput improvement.

Appendix 1: Hardware setup

The hardware setup overview is given in Figure 24.

1.1 System overview

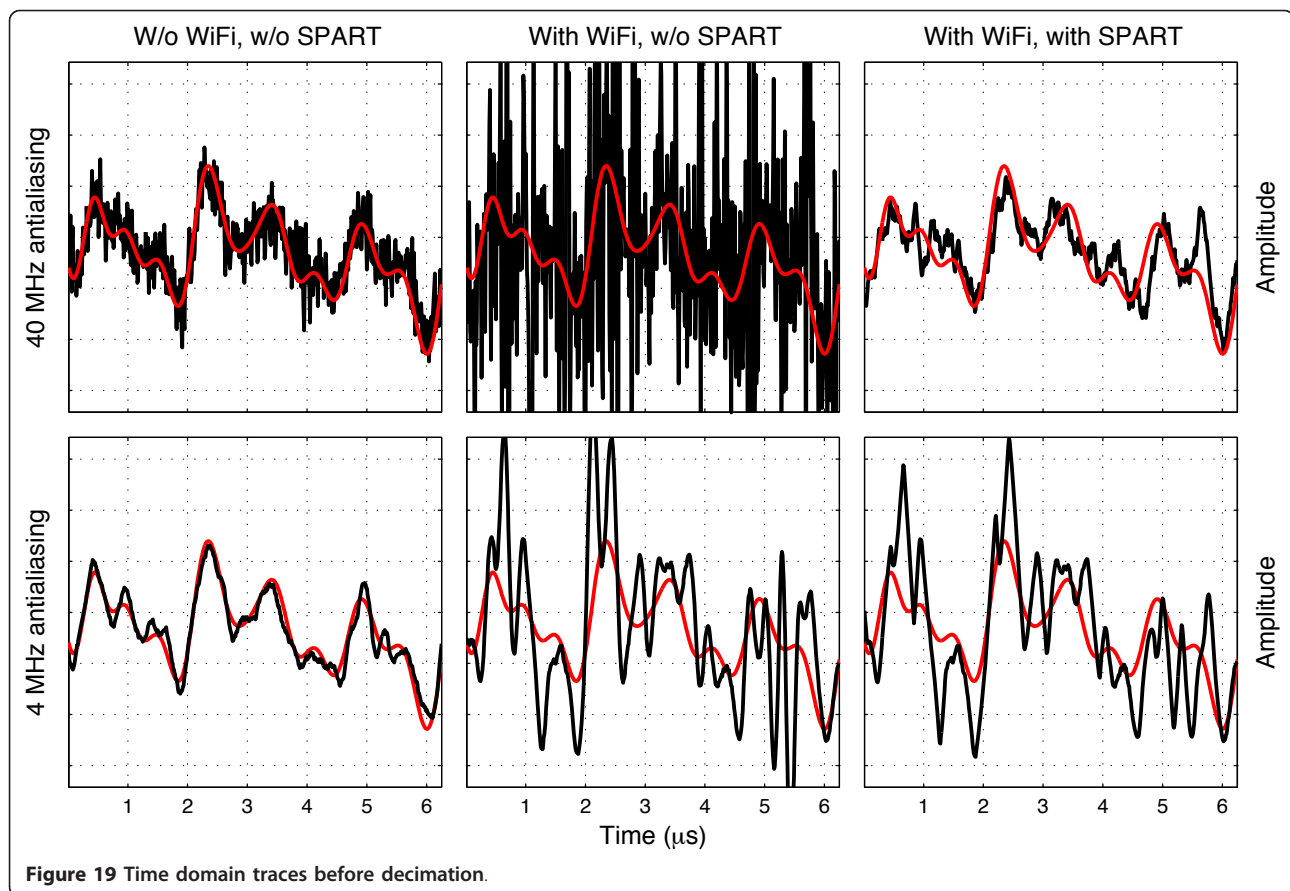
The measurement system consists of the N210/DBSRX2 receiver combination inside of an RF shielded enclosure. The enclosure allows entry of the HSDPA, WiFi, 10 MHz reference clock, and 1 pulse per second (PPS) timing signal through SubMiniature version A (SMA) connectors in the side of the enclosure. Power and Ethernet connections pass through a ferrite toroid just outside of the enclosure, and into the enclosure to connect to the N210. The 10 MHz reference clock and 1 PPS timing signal pass through a separate ferrite toroid. Also contained inside of the RF enclosure are the RF splitter/combiner, the common path attenuator, the WiFi band-stop filter, and the HSDPA preselect filter.

The USRP2/WBX HSDPA and the USRP2/XCVR2450 WiFi signal sources are located outside of the RF enclosure. The HSDPA signal to the receiver passes through a series of passive attenuators that are attached to the SMA connector outside of the enclosure. All RF signals are routed via UT-141 semi-rigid coaxial cables.

Also located outside of the enclosure is the 10 MHz timebase and the 1 PPS signal source. These signals are used for time and phase synchronization between the signal sources and the receiver. The synchronization was used to enable concatenation of the received data samples together, since data was collected at a 100 MS/s rate until N210 SRAM memory was full, and then transferred to the host computer over the Ethernet connection.

1.2 SDRs

The SDRs from Ettus Research [9,10] were chosen for the test platform due to their availability, frequency coverage, documentation availability, and ease of use. Each SDR consists of a base unit that contains two 100 MS/s ADCs, two 400 MS/s DACs, post-ADC FPGA processing, and interface circuitry. The analog portions of the transmitters and receiver are contained on



daughterboards that plug into the base unit. All hardware, firmware, and software are open source with full schematics available for the base units and the daughterboards.

1.3 HSDPA transmitter

This signal source consists of a USRP2 base unit, and a WBX daughterboard. The WBX daughterboard has signal generation capability from 50 MHz to 2.2 GHz. I/Q modulation is provided by the USRP2 DAC converters. Data interface to the USRP2 is provided via a gigabit Ethernet connection. The WBX and USRP2 hardware used for the HSDPA transmission is unmodified.

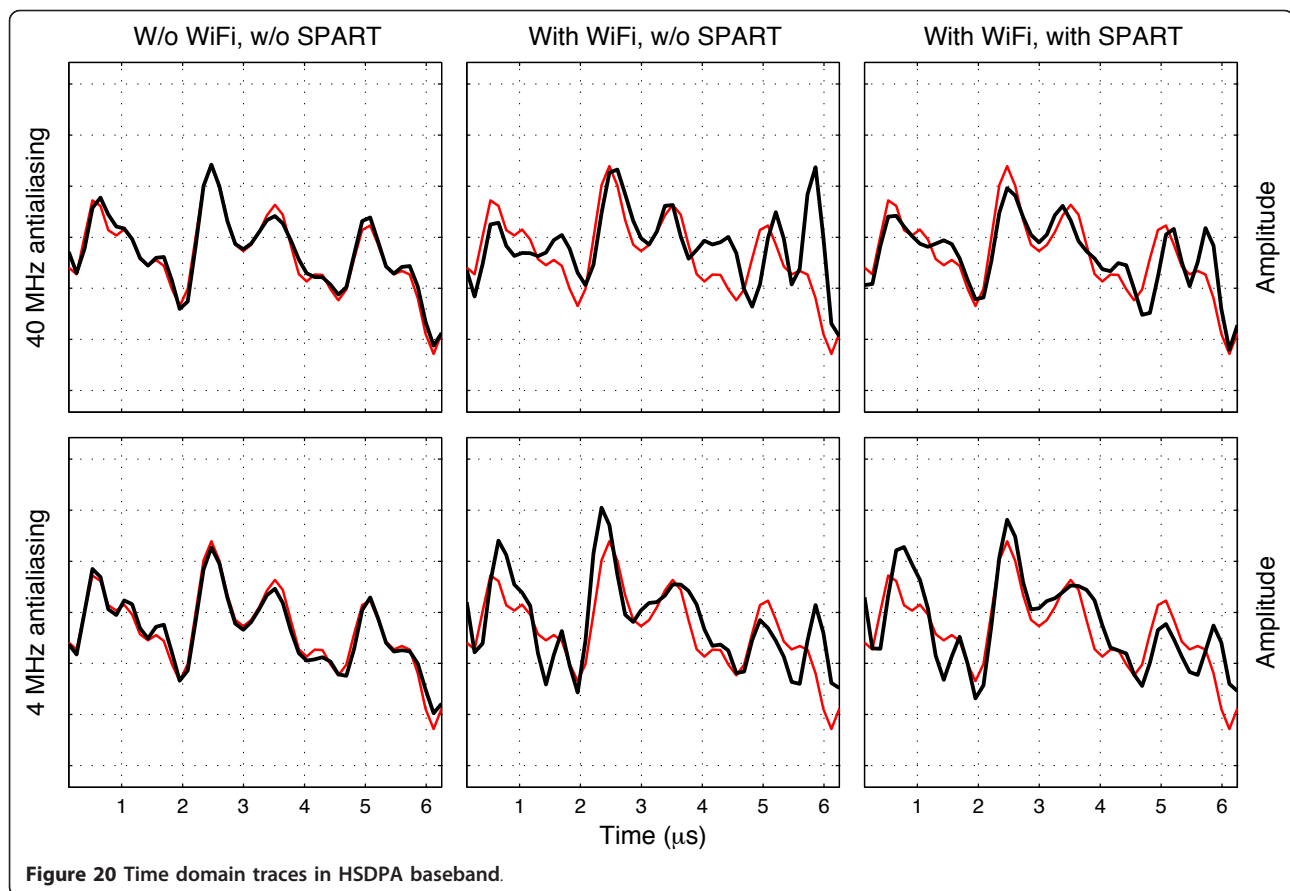
1.4 WiFi transmitter

This signal source consists of a USRP2 base unit, and a XCVR2450 daughterboard. The daughterboard has signal generation and reception capability from 2.4 to 2.5 GHz, and from 4.9 to 5.9 GHz. I/Q modulation is provided by the USRP2 DAC converters. Data interface to the USRP2 is provided via a gigabit Ethernet connection. The receiver portion of this daughterboard is not used in the tests. The XCVR2450 and USRP2 hardware used for the WiFi transmission is unmodified.

1.5 HSDPA receiver

This receiver consists of a USRP N210 base unit, and a DBSRX2 daughterboard. The daughterboard has signal reception capability from 800 MHz to 2.4 GHz. The I/Q receiver outputs are supplied to the N210 ADC converters. Data interface to the N210 is provided via a gigabit Ethernet connection. Moderate modifications were made to the DBSRX2 daughterboard [24] <http://code.ettus.com/redmine/ettus/attachments/88/dbsrx2.pdf> to reduce spurious signals, most of which appear to be generated by the N210 circuitry and the 100 and 25 MHz reference clocks.

- (1) *Bypassing* . Additional 100 nF 1.6 × 0.79 mm (0603-size) surface-mount capacitors have been placed in parallel with 1 nF capacitors C74, C75, and C76.
- (2) *Shielding* . The DBSRX2 has an on-board divide-by-4 prescaler that divides the 100 MHz reference clock to 25 MHz before applying the reference signal to the receiver PLL. An RF shield was constructed to reduce the noise coupled into the receiver, and to add isolation from the clock signals.



1.6 Antialiasing filter

The MAX2112 IC used in the DBSRX2 daughterboard [24] has an internal antialiasing filter following the mixer, which is a 7th order Butterworth lowpass filter with the 3 dB corner frequency programmable between 4 and 40 MHz. This internal filter is followed by an external lowpass filter with 3 dB roll-off frequency of approximately 33 MHz.

1.6.1 Antialiasing filter modification

To increase the bandwidth of the IF anti-aliasing filters (both I and Q), capacitors C66, C67, C85, and C86 were removed from the circuit, and 100 pF capacitors C25, C26, C64, and C65 were replaced with 33 pF capacitors. These modifications increased the 3 dB roll-off frequency of the external antialiasing filter to about 45 MHz, which allowed us to utilize the full programmable range of the internal antialiasing filter.

1.7 Preselect and bandstop filters

The preselect filter was constructed using three Panasonic EFCH1950TCD1 SAW filters in a small shielded enclosure. A shield was placed in the enclosure for each SAW filter, with the shield placed perpendicular to the signal flow on top of the SAW package. This helps to

isolate the signal between the input and output of each filter, and to improve the ground for each SAW device. Input and output ports for the preselect filter are SMA connectors. Figure 25 shows the measured response of the preselect filter.

The WiFi bandstop filter is constructed using three coaxial resonator elements. The elements are $\lambda/8$ (open), and are made from UT-141 semi-rigid coaxial cable. Figure 26 shows the measured response of the WiFi bandstop filter.

1.8 Timebase

The timebase generates a 10 MHz reference clock and 1 PPS signal used for time and frequency synchronization of the transmitters and the receiver. The accurate and common reference allows reconstruction of received data from multiple 100 MS/s data packets. The 10 MHz reference is generated by a Temperature-Compensated Crystal Oscillator (TCXO), and is within 0.25 PPM of the nominal frequency. A Peripheral Interface Controller (PIC) microprocessor is used to generate the 1 PPS signal derived from the 10 MHz reference. This signal is generated using the internal counter, and software to count cycles of the reference clock and drive an output

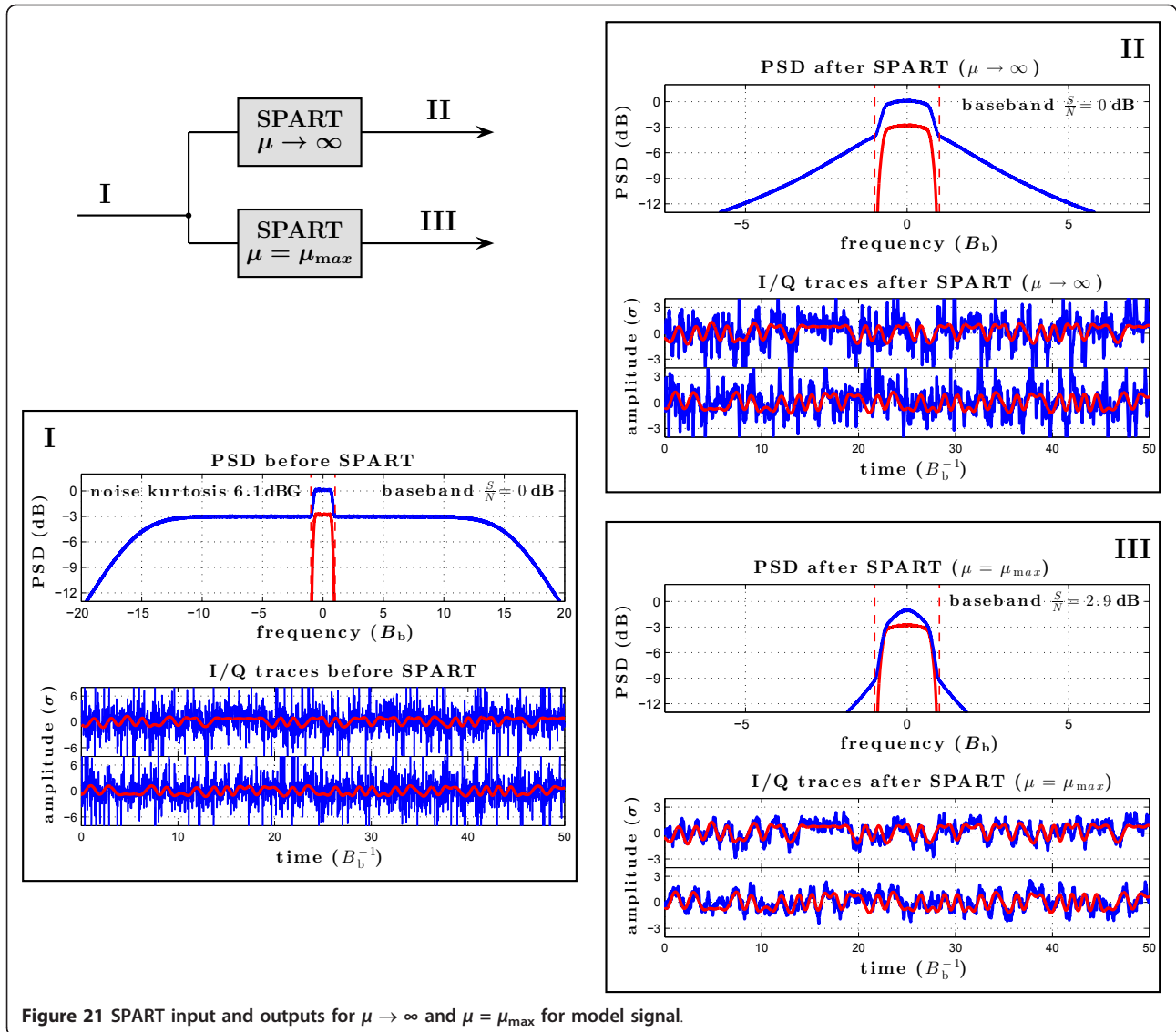


Figure 21 SPART input and outputs for $\mu \rightarrow \infty$ and $\mu = \mu_{max}$ for model signal.

pin based on the reference time and phase. Both the 10 MHz and 1 PPS reference signals are buffered, with a three-output passive splitter forming the load for each output buffer.

Appendix 2: Complex-valued SPART filter

The SPART filter used in this article is defined as the following feedback circuit [6]:

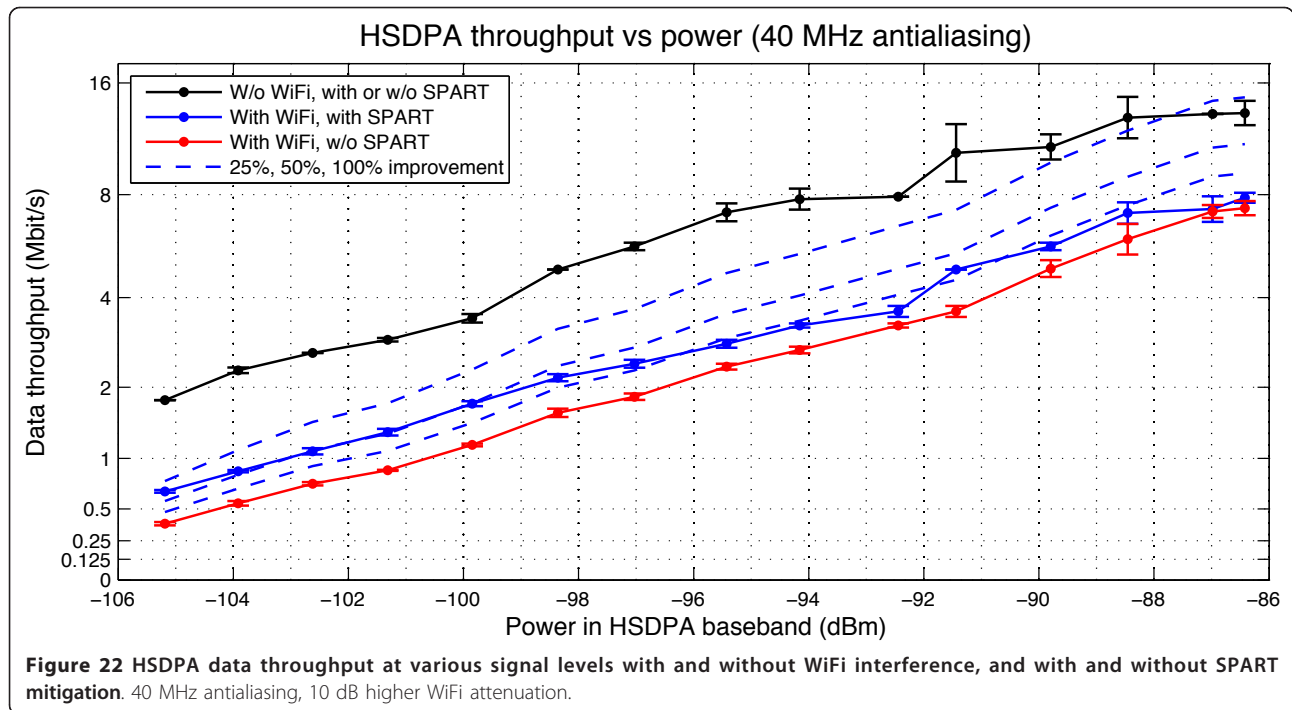
$$\zeta(\mu, \tau)(t) = \mu \int dt \left\{ \tilde{\mathcal{F}}_{\mu\tau}[z(t) - \zeta(\mu, \tau)(t)] \right\}, \quad (1)$$

where $z(t)$ is the (complex-valued) input signal, $\zeta(\mu, \tau)(t)$ is the output, μ and τ are positive *rate parameter* and *time constant*, respectively, and $\tilde{\mathcal{F}}_{\alpha}(z)$ is a *comparator* function with the resolution (linear range) parameter α . In this study, the following comparator function was

used:

$$\tilde{\mathcal{F}}_{\alpha}(z) = \frac{z}{|z|} \tilde{\mathcal{F}}_{\alpha}(|z|) = \frac{z}{|z|} \begin{cases} \frac{|z|}{\alpha} & \text{for } |z| < \alpha \\ 1 & \text{otherwise} \end{cases}. \quad (2)$$

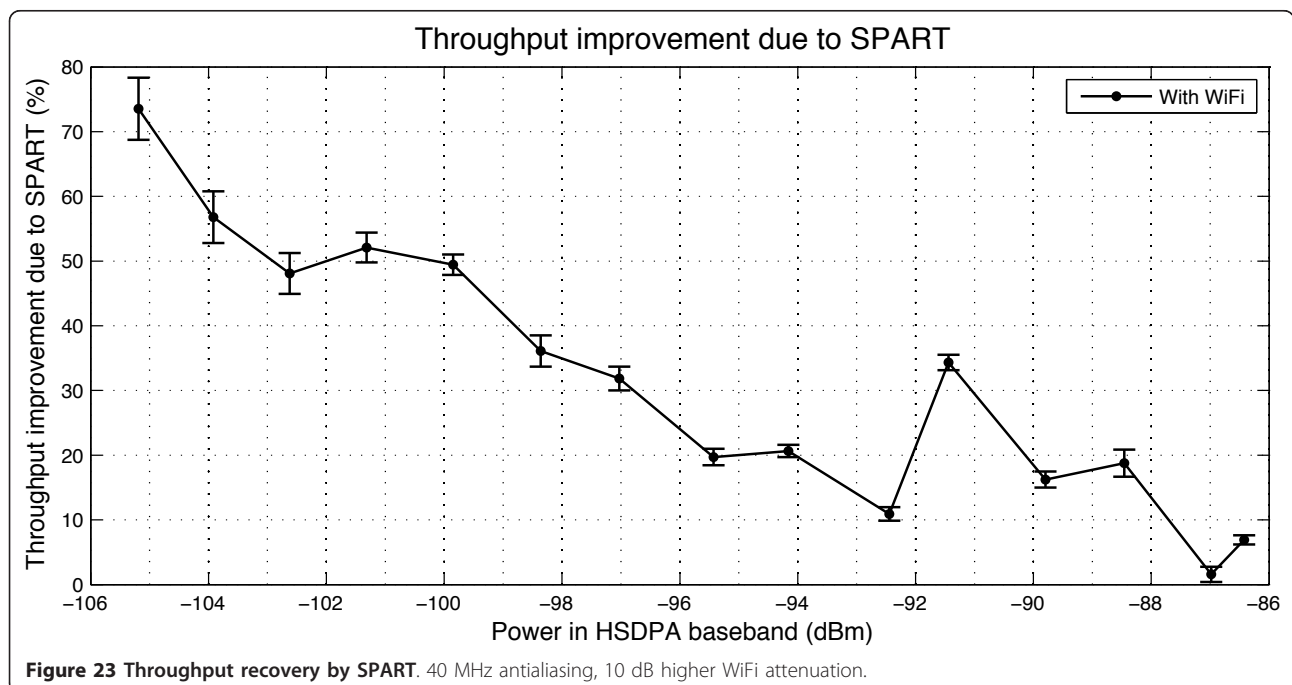
When the condition $|z(t) - \zeta(\mu, \tau)(t)| < \mu\tau$ is satisfied, the response of the circuit equals that of a 1st order (one-pole) lowpass filter having the same time constant τ . Otherwise, while having the same *sign* (real and/or complex), the absolute value of the rate of change of the output is smaller than the one of the lowpass filter. If a SPART circuit with sufficiently small τ is deployed early in the signal chain of a receiver channel affected by non-Gaussian impulsive noise, it can be shown that there exists such rate parameter μ that maximizes SNR and improves the quality of the channel. Figure 27 provides an illustration of this statement.



This figure shows that, when viewed as a function of the rate parameter μ , for any noise composition the channel quality measured by the average baseband SNR asymptotically approaches a constant value in the limit of large μ . If the noise is purely thermal (Gaussian), for sufficiently large values of μ the average SNR monotonically increases while approaching this asymptotic value

(dashed line in the figure). If, however, the total noise is impulsive and contains relatively short duration “bursts” of relatively high power, the average SNR exhibits an absolute maximum at some finite value of the rate parameter μ_{\max} (solid line).

In Figure 21, the blue lines show the PSDs and the time domain traces of the input and the outputs of a



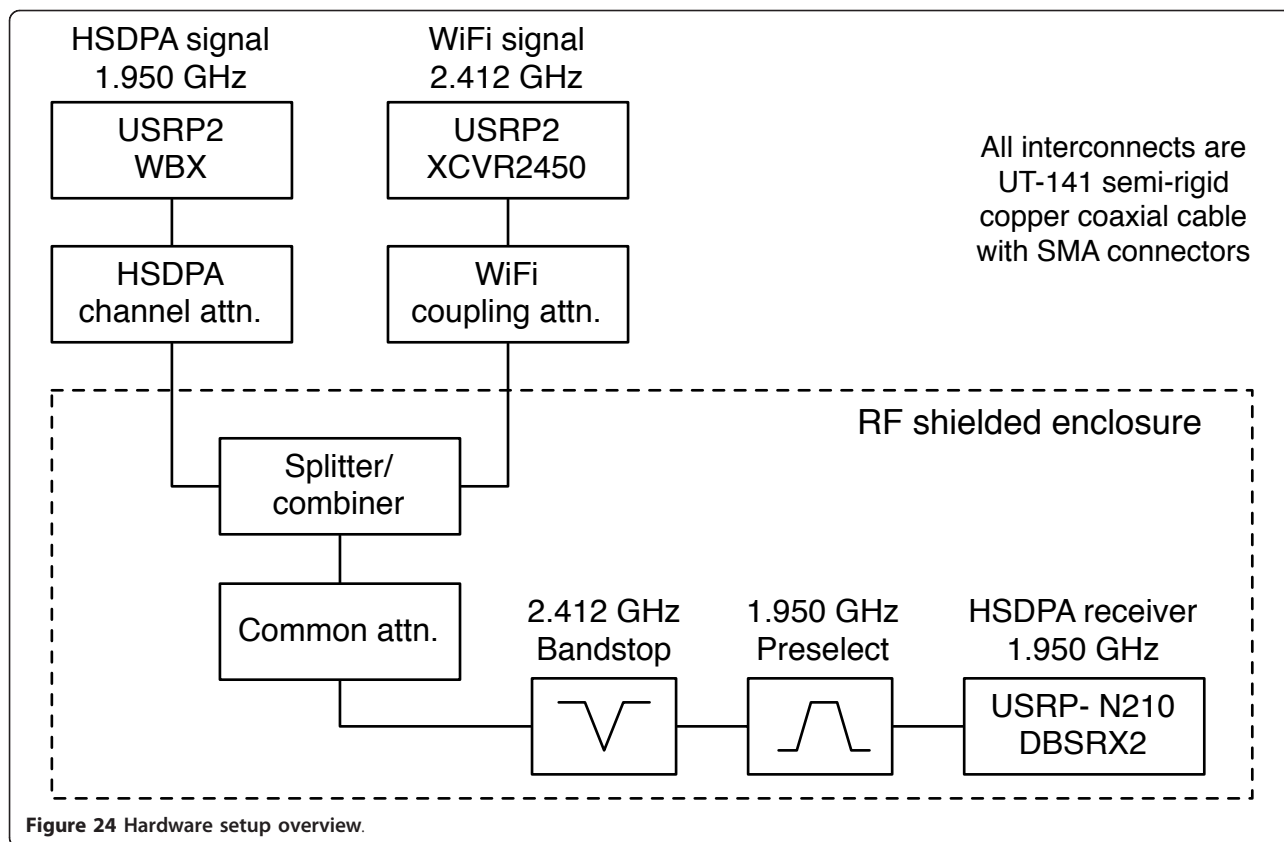


Figure 24 Hardware setup overview.

SPART filter applied to a model signal+noise mixture with the characteristics (the noise bandwidth and kurtosis, and the SNR) similar to those encountered in the experiment presented in this study. The outputs of the

SPART filter are shown for the cases of a large rate parameter ($\mu \rightarrow \infty$, panel II), and the rate parameter $\mu = \mu_{\max}$ that maximizes the SNR in the baseband (panel III). For reference, the respective PSDs and the time

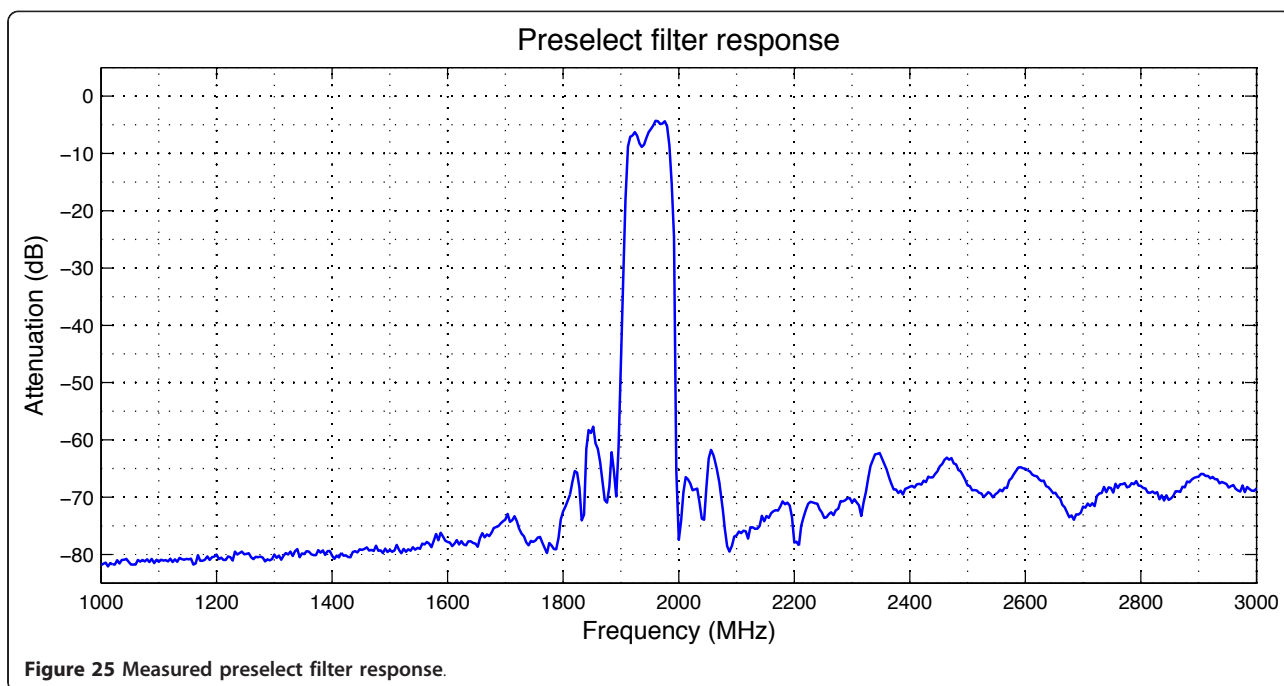
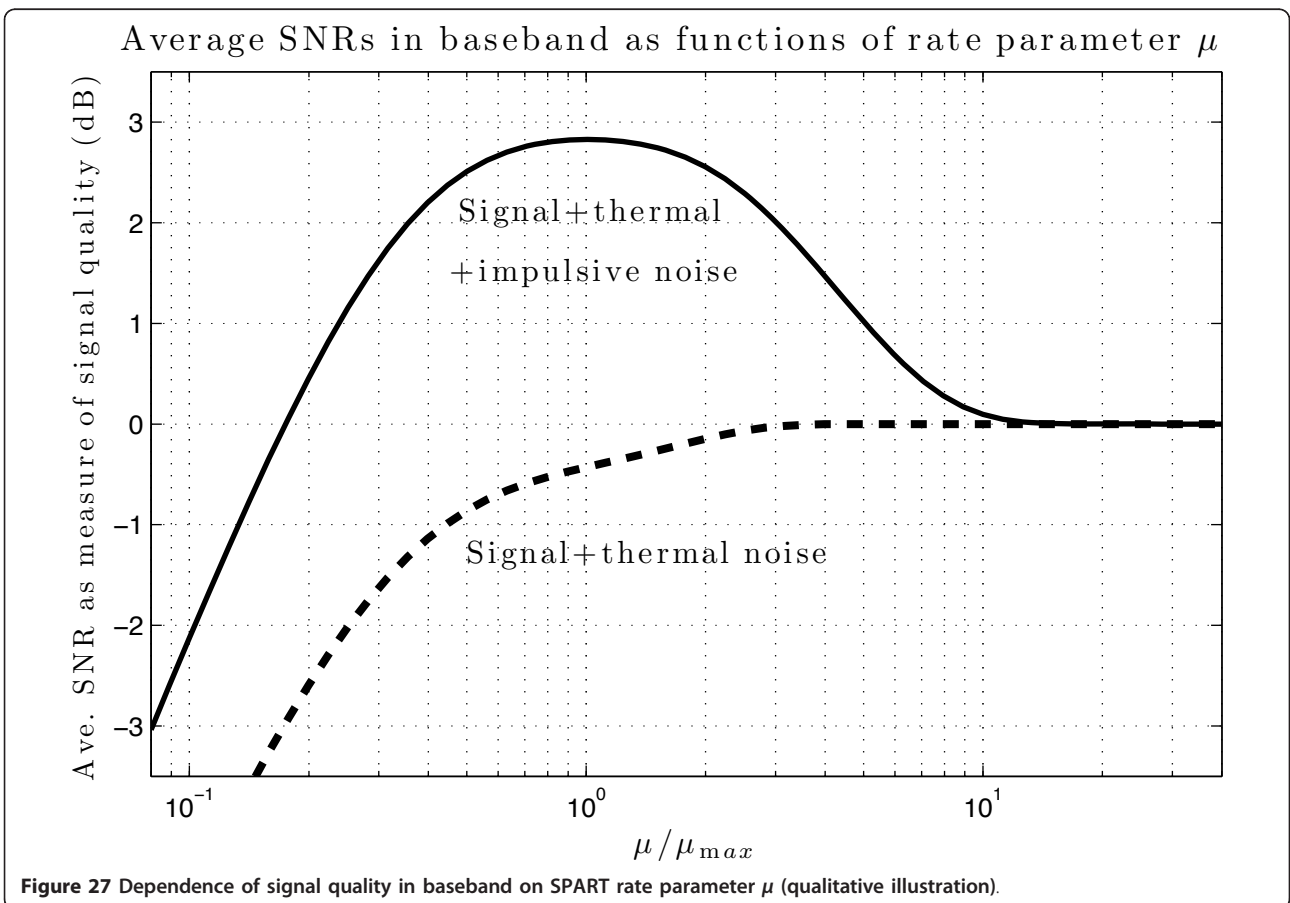
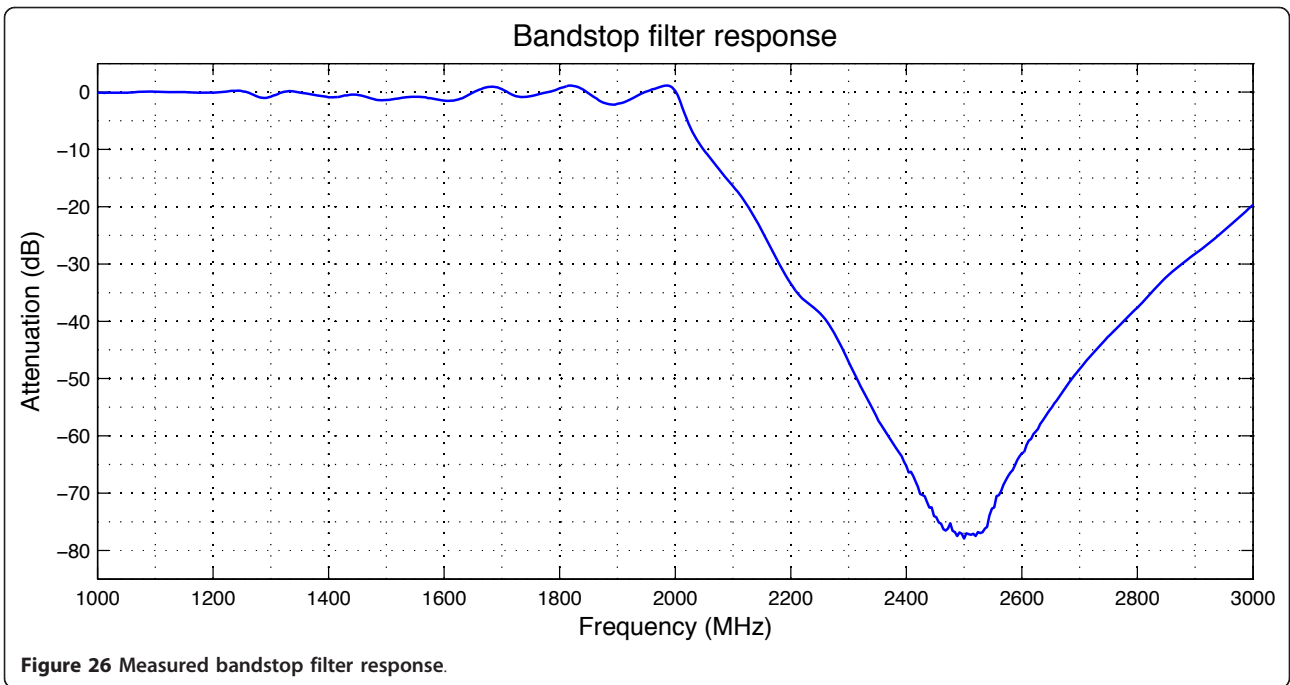


Figure 25 Measured preselect filter response.



domain traces for the signal without noise are shown by the red lines.

The time constant τ of the SPART filter used in the example is relatively small, $\tau = 1/(4\pi B_b)$, and in the limit of a large rate parameter ($\mu \rightarrow \infty$) the SPART filter is a linear 1st order lowpass filter with the 3 dB roll-off frequency $2B_b$. As can be seen in panel II, this filter does not noticeably affect the SNR in the baseband of interest (it remains 0 dB) as it only reduces the higher-frequency noise.

If we start reducing the rate parameter, “trimming” of the short-duration, high-power outliers comes into effect before the reduction in the rate parameter affects the narrower- bandwidth trend in the signal. If the noise contains such outliers (that is, the noise is impulsive), the value $\mu = \mu_{\max}$ produces the maximum in an appropriate measure of the signal quality, for example, in the baseband SNR. This can be seen in panel III of Figure 21. The time domain traces show that the SPART filter with $\mu = \mu_{\max}$ reduces the impulsive noise by “trimming” the outliers while following the narrower-bandwidth trend in the signal, and the PSD plot shows that the noise floor is reduced throughout the full frequency range (including the baseband), leading to the 2.9 dB increase in the baseband SNR.

The example presented in Figure 21 should be qualitatively compared with the experimental data shown in Figures 16, 17, and 19. In particular, the PSD plots in panels I, II, and III correspond to the PSDs shown in the upper right panel of Figure 16, and in the upper middle and the upper right panels of Figure 17, respectively. Also, the time domain traces shown in panels I and III correspond to the time domain traces of the upper middle and the upper right panels of Figure 19, respectively.

2.1 Digital SPART

An example of a numerical algorithm implementing a finite-difference version of a SPART filter is given by the following MATLAB function:

```
function zeta = SPART(z, t, mu, tau)
zeta = zeros(size(z));
dt = diff(t);
alpha = mu*(tau+dt);
zeta(1) = z(1);
for i = 2:length(z);
    FF = z(i)-zeta(i-1);
    if abs(FF) < alpha(i-1)
        FF = FF/alpha(i-1);
    else
        FF = FF/abs(FF);
    end
    zeta(i) = zeta(i-1) + mu*FF*dt(i-1);
```

```
end
return
```

One can see that a digital SPART is computationally inexpensive and requires very little memory, which makes it suitable for real-time implementation in FPGA and/or software.

Appendix 3: Calibration, power levels, and noise floor

3.1 WiFi power

Figure 28 shows the PSD of the transmitted WiFi signal measured by the Advantest R3131A spectrum analyzer at the output of the XCVR2450 daughterboard. The vertical red lines indicate the bandwidth (16.8 MHz) used for calculating the total transmitted power of 50 mW (17 dBm).

3.2 HSDPA transmission

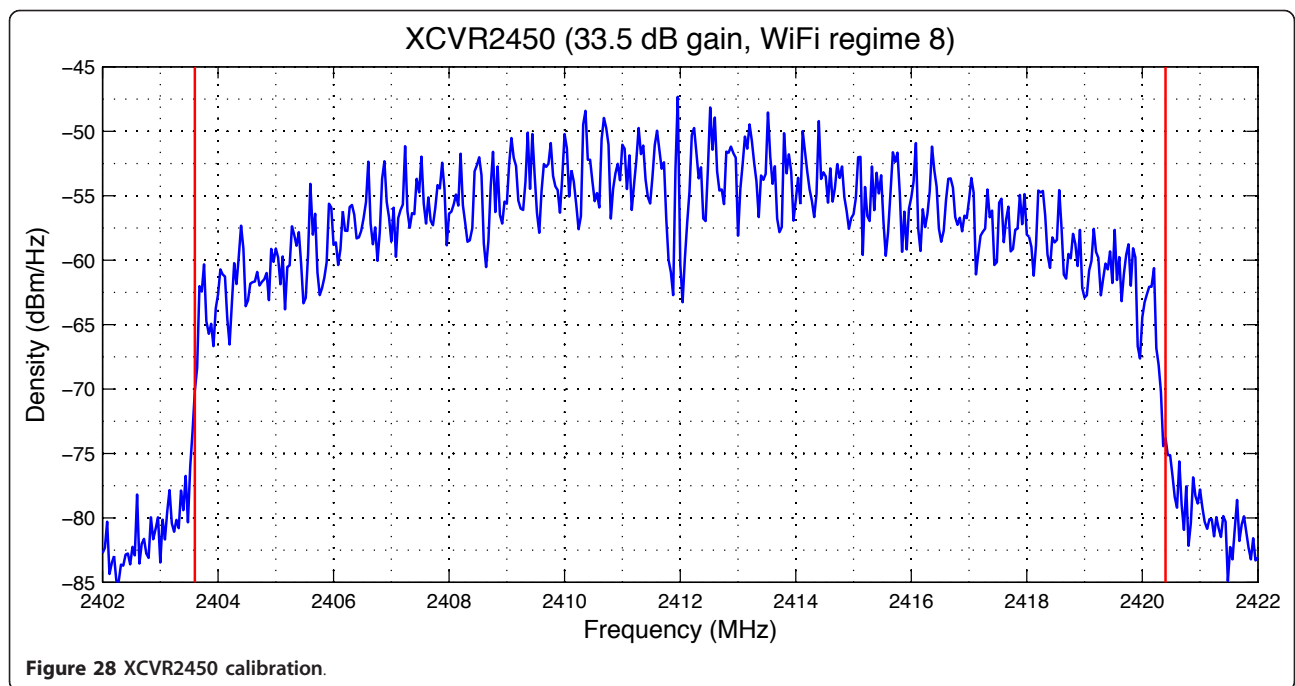
Figure 29 shows the total power of the HSDPA signal for different modulations, transmitted by the WBX daughterboard and measured by the Advantest R3131A spectrum analyzer in the HSDPA band (4.8 MHz), as functions of the transmitter gain settings ('Tx gain'). One can see that the usable power range of the WBX transmitter is -18 to 2.6 dBm.

All measured losses at 1.95 GHz due to the connectors, cables, and attenuators amount to approximately 83 dB, and the total insertion losses of the bandstop and preselect filters at 1.95 GHz are measured to be 7 dB. This leads to the expected HSDPA power at the receiver input to be from -108 to -87.4 dBm.

3.3 Received signal and noise

The transmit power calibration data shown in Figure 29 allows us, after applying all losses due to the connectors, cables, and attenuators (83 dB), and the insertion losses of the bandstop and preselect filters (7 dB), to calculate the expected HSDPA power at the receiver input. We then measure the powers of the noise with and without the OOB WiFi, and the powers of the signal + noise mixtures, and equate the measured powers of the signal + noise mixtures with the respective sums of the measured noise and the expected HSDPA power. This allows us to verify the calibration of the measured power in the receiver, determine the receiver noise figure, and measure the noise floor.

Figures 30 and 31 plot the measured powers for the noise and the signal + noise mixtures for the cases with and without WiFi interference, as functions of the HSDPA power expected from the transmitter gain settings, and compare them with the expected HSDPA power, and the respective sums of the measured noise and the expected power. One can see in both figures



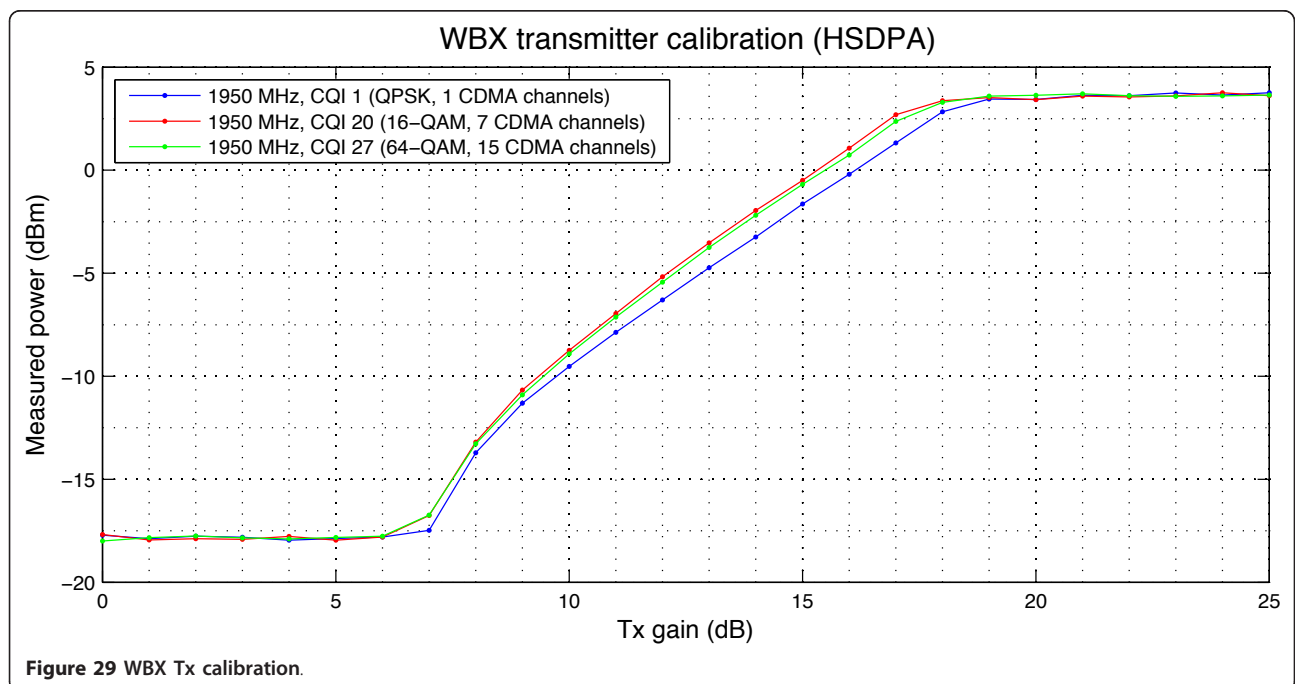
that the -104 dBm noise level without WiFi corresponds well with the -177 dBm/Hz thermal noise level at room temperature, measured in the 4.8 MHz HSDPA pass-band (67 dB), plus the 6 dB receiver noise figure.

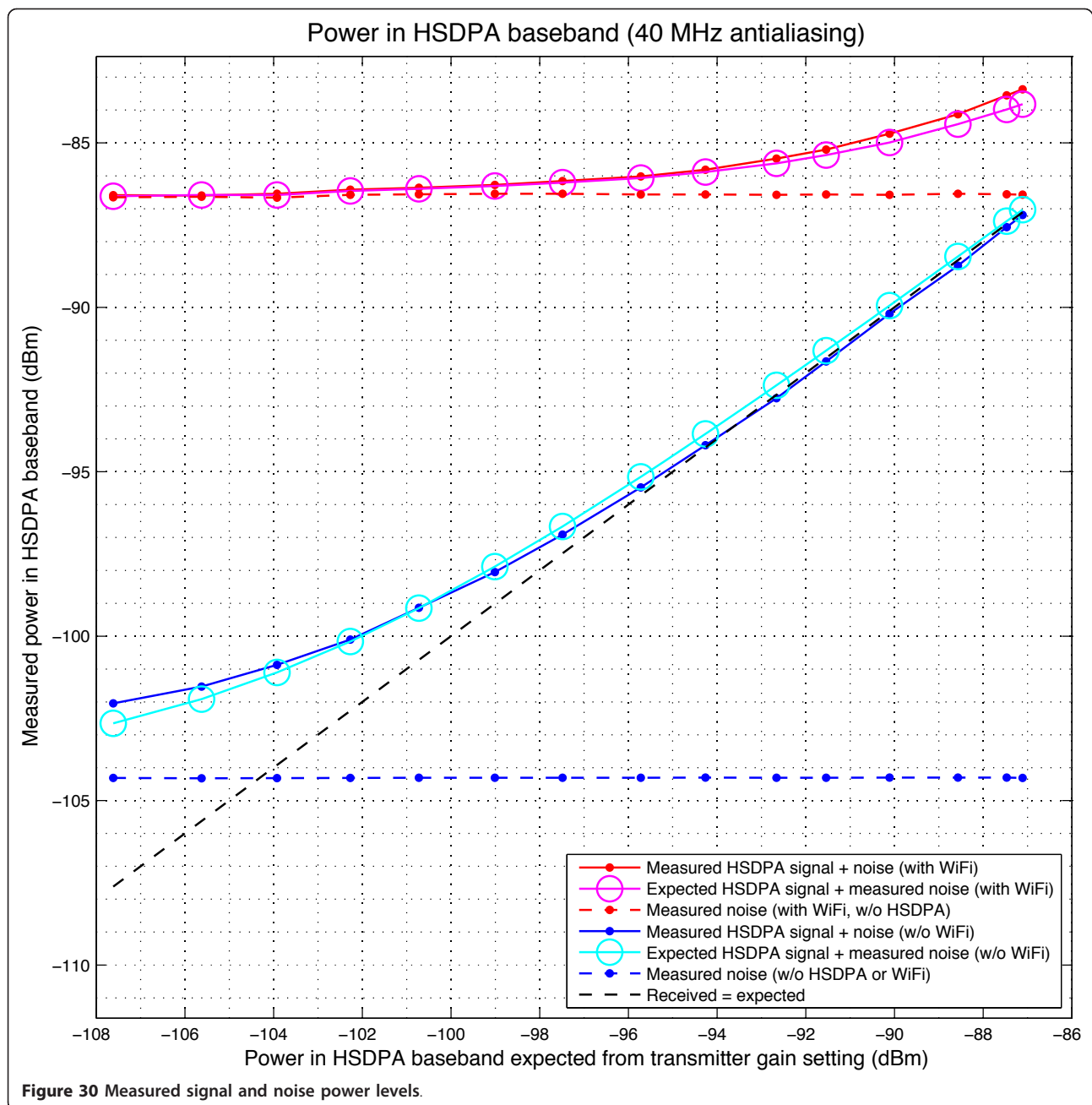
In Figure 30, the OOB WiFi contributes 17 dB into the rise in the noise level, while in Figure 31 it contributes approximately 8 dB. In both figures, the measured

signal + noise levels correspond to the respective sums of the respective measured noise levels and the expected signal power.

3.4 ADC saturation

Figure 32 plots the fraction of the ADC samples, for the case of 40 MHz antialiasing, with the absolute value in





either I or Q at the maximum ADC value. The ADC saturation during WiFi transmission is caused by the high amplitude outliers.

There is no ADC saturation when 4 MHz antialiasing and/or a 10 dB lower WiFi power is used.

Appendix 4: Software

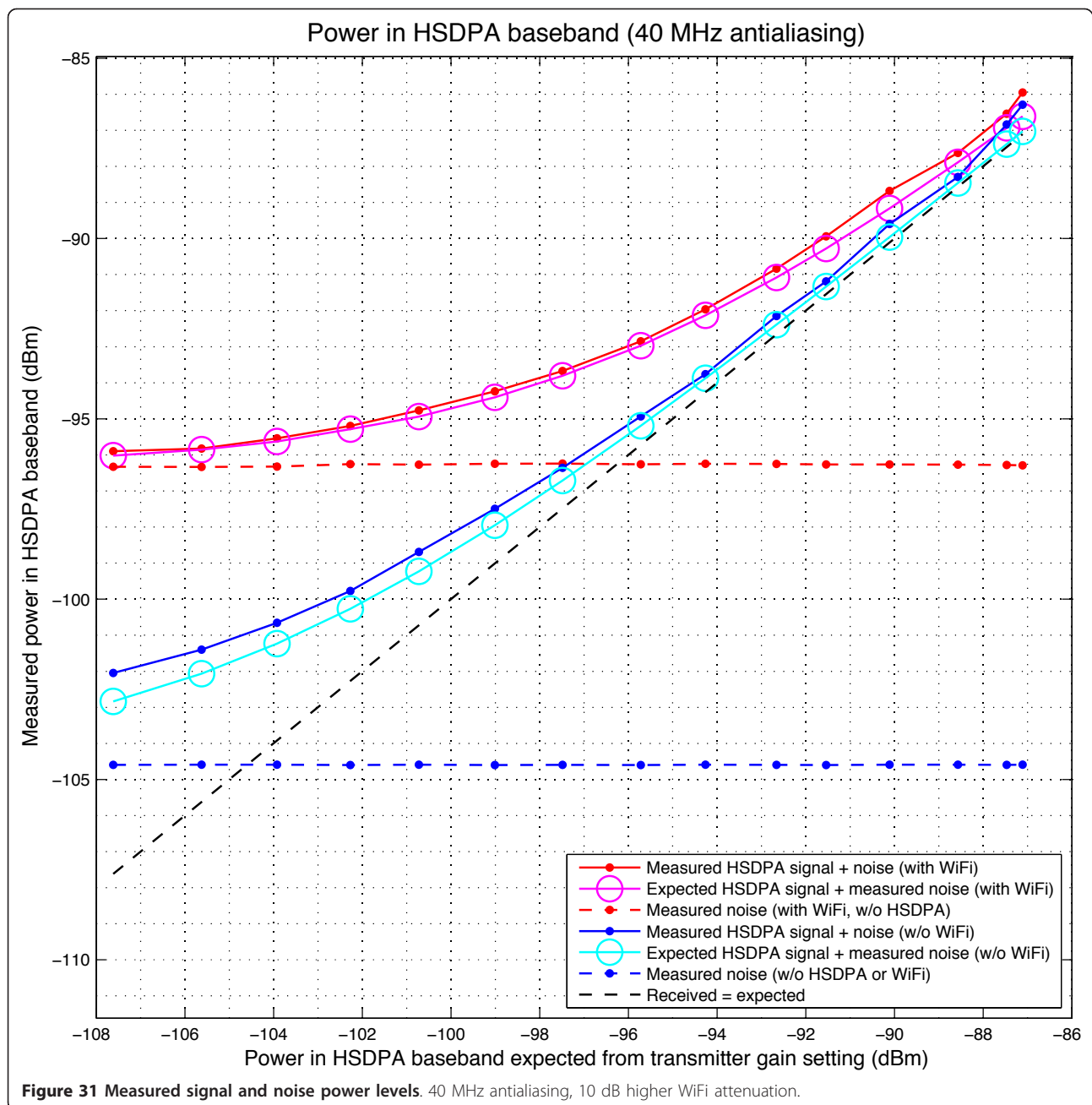
4.1 Overview

The main software of this experiment is implemented in MATLAB, version R2009b. The SDR, HSDPA, and WiFi

software/firmware are based on open source projects that are described below.

4.2 Software-defined radios

The software-defined radios are controlled with Ettus Research Universal Hardware Driver (UHD) [11]. The UHD is a device driver and an application programming interface (API) for controlling the SDRs used in the experiment. In our implementation, the UHD is extended to allow 100 MS/s data collection used in



direct comparison between the original signal, and the filtered SPART signal.

4.3 HSDPA

Much of the physical layer of the HSDPA channel is performed in the Iterative Solutions' Coded Modulation Library (CML) version 1.0 [18] <http://www.iterativesolutions.com/Matlab.htm>. CML is used to implement the Hybrid Automatic Repeat reQuest (HARQ), and the constellation mapping in our test. HARQ is forward error correction coding combined with error detection,

that determines if retransmission due to a block error is needed in a transmitted HSDPA data frame. Variable data throughput is executed in HSDPA through Adaptive Modulation and Coding (AMC) by altering the modulation scheme, and the puncturing of parity bits.

4.3.1 CQI mapping table

The throughput of the channel is mapped to CQI. The CQI mapping table used in testing is based on 3GPP 25.214 table 7G [[17], p. 61], and is shown in Figure 1. 64-QAM capability was added to the CML to allow the use of higher CQI values.

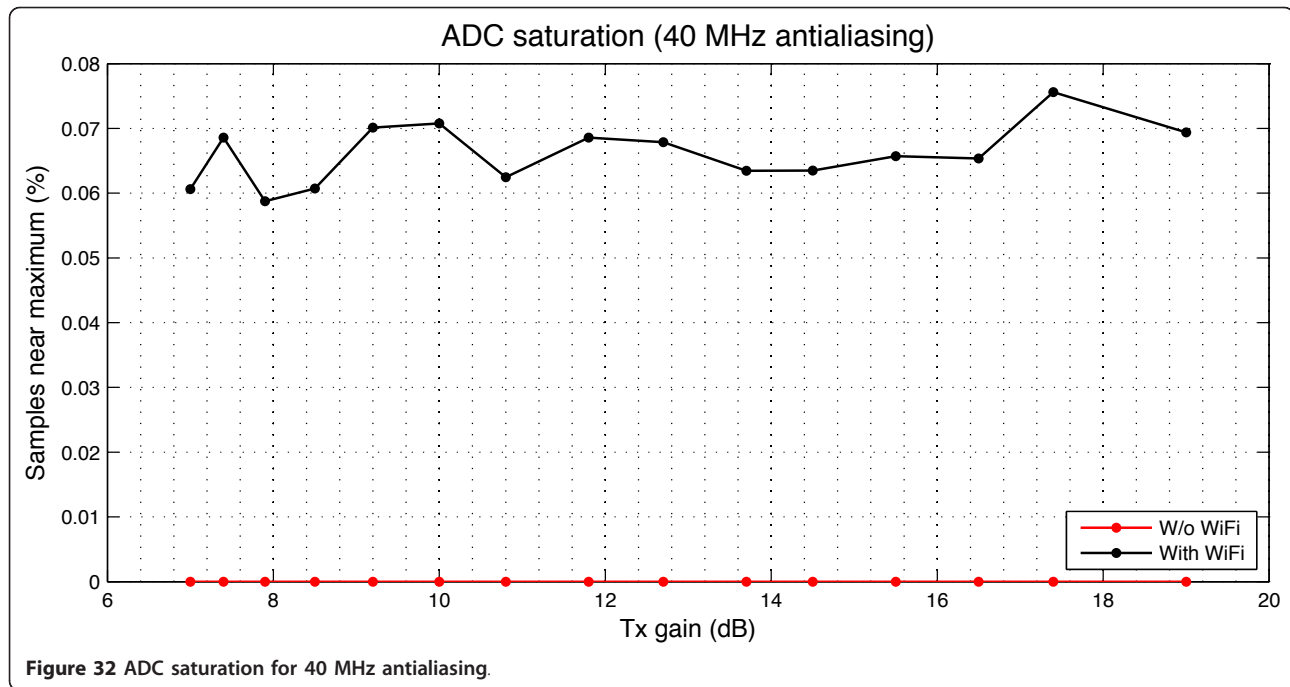


Figure 32 ADC saturation for 40 MHz antialiasing.

4.4 WiFi

For the WiFi transmission, we use the FTW 802.11 package for GNU Radio [19] <http://gnuradio.org/redmine/> to pre-compute standard 802.11 g frames to be sent to a USRP2 for transmission by the XCVR2450 daughterboard. This software stack can be used to implement 802.11 g by interpolating the signal by a factor of 5 in the USRP2. The encoder has been tested with Atheros, Ralink, Intel, and Broadcom chipsets to decode the frames sent through a similarly configured SDR <https://www.cgran.org/wiki/ftw80211ofdm#ProjectDescription>. The message sent by the interfering WiFi transmitter is an 802.11 g reference frame transmitted at 54 Mbit/s, which is the maximum data rate supported by 802.11 g.

Endnotes

^aIn [6], the SPART filter used in this article is referred to as 'FrankenSPART'. A detailed description and examples of the performance of other analog nonlinear filters for impulsive noise mitigation can be found in [5,7]. ^bBased on our bench measurements for small antennas separated by approximately 3.5 inches, and on the reported -13 to -30 dB mutual coupling between MIMO antennas of similar types and separation [22,23], 15 dB (about 30 times) WiFi attenuation at 1.95 GHz, while representing a relatively strong WiFi and HSDPA antenna coupling at the HSDPA frequency, is within practically encountered range. Also, since our WiFi transmit power is almost an order of magnitude lower than the conducted WiFi power found in many real life devices, this coupling

attenuation can be assumed to be over 20 dB. ^cThe ADC saturation is briefly discussed in Sections 2.4.1 and 4.1, and in Section "ADC saturation" of Appendix 3.

Abbreviations

3GPP: 3rd Generation Partnership Project; ADC: Analog-to-Digital Converter; AMC: Adaptive Modulation and Coding; API: Application Programming Interface; AWGN: Additive White Gaussian Noise; BER: Bit Error Rate, or Bit Error Ratio; CDMA: Code Division Multiple Access; CQI: Channel Quality Indicator; CML: Coded Modulation Library; CRC: Cyclic Redundancy Code; DAC: Digital-to-Analog Converter; dBm: dB per milliwatt; FDD: Frequency Division Duplexing; FFT: Fast Fourier Transform; FIR: Finite Impulse Response; FPGA: Field Programmable Gate Array; FTW: Forschungszentrum Telekommunikation Wien (The Telecommunications Research Center Vienna); GNU: "GNU's Not Unix!(recursive acronym); GPS: Global Positioning System; HARQ: Hybrid Automatic Repeat reQuest; HDL: Hardware Description Language; HSDPA: High Speed Downlink Packet Access; IC: Integrated Circuit; IF: Intermediate Frequency; I/Q: In-phase/Quadrature; LNA: Low-Noise Amplifier; MATLAB: MATrix LABoratory; Mbit/s: megabit per second; MIMO: Multiple-Input and Multiple-Output; MS/s: million of samples per second; NDL: Nonlinear Differential Limiter; OFDM: Orthogonal Frequency Division Multiplexing; OOB: OutOf-Band; PIC: Peripheral Interface Controller; PLL: Phase-Locked Loop; PPM: Parts Per Million; PPS: Pulse Per Second; PSD: Power Spectral Density; QAM: Quadrature Amplitude Modulation; QPSK: Quadrature Phase-Shift Keying (4-QAM); RAM: Random-Access Memory; RF: Radio Frequency; RRC: Root Raised Cosine; SAW: Surface Acoustic Wave; SDR: Software Defined Radio; SMA: SubMiniature version A; SNR: Signal to Noise Ratio; SPART: Single Point Analog Rank Tracker; SRAM: Static Random-Access Memory; TCXO: Temperature-Compensated Crystal Oscillator; TTI: Transmission Time Interval; UARFCN: UTRA Absolute Radio Frequency Channel Number; UHD: Universal Hardware Driver; UMTS: Universal Mobile Telecommunications System; UTRA: UTRA Terrestrial Radio Access; WCDMA: Wideband Code Division Multiple Access; WiFi: Wireless Fidelity (a branded standard for wirelessly connecting electronic devices).

Acknowledgements

The authors express their sincere appreciation to Ruslan L Davidchack of the University of Leicester, United Kingdom, to David A Johnson of Pinnacle

Technology Inc., USA, and to Rashidus Mia of TruePosition Inc., USA, for their valuable suggestions and critical comments.

Author details

¹Avatekh Inc., 900 Massachusetts Street, Suite 409, Lawrence, KS 66044, USA

²Horizon Analog Inc., 10 East 9th Street, Suite G, Lawrence, KS 66044, USA

Competing interests

The authors declare that they are stockholders in the listed companies of their affiliation, and had financial support from Avatekh Inc. and Horizon Analog Inc. for the submitted work. Horizon Analog Inc. is an associate company of Avatekh Inc. The ongoing results and source materials of the submitted work, prior to submission and/or publication, have been shared under mutual nondisclosure agreements with a major US wireless carrier and with two major IC manufacturers. The authors have no other relationships or activities that could appear to have influenced the submitted work.

Received: 24 September 2011 Accepted: 10 April 2012

Published: 10 April 2012

References

1. K Slattery, H Skinner, *Platform Interference in Wireless Systems*, (Elsevier, Amsterdam, 2008)
2. F Leferink, F Silva, J Catrysse, S Batterman, V Beauvois, A Roc'h, Man-made noise in our living environments. *Radio Sci Bull.* **334**, 49–57 (2010)
3. X Yang, A Petropulu, Co-channel interference modeling and analysis in a Poisson field of interferers in wireless communications. *IEEE Trans Signal Process.* **51**, 64–76 (2003)
4. AV Nikitin, On the impulsive nature of interchannel interference in digital communication systems, in *Proc IEEE Radio and Wireless Symposium*, Phoenix, AZ, pp. 118–121 (2011)
5. AV Nikitin, On the interchannel interference in digital communication systems, its impulsive nature, and its mitigation. *EURASIP J Adv Signal Process.* **2011**, 137 (2011)
6. AV Nikitin, Method and apparatus for adaptive real-time signal conditioning and analysis, US Patent Application Publication 2011/0112784. (12 May 2011)
7. AV Nikitin, Analog nonlinear differential limiters, US patent pending 61/573,305. (2 Sept 2011)
8. 3rd Generation Partnership Project; Technical Specification Group Radio Access Network; High Speed Downlink Packet Access (HSDPA); Overall description; Stage 2 (Release 9) <http://www.quintillion.co.jp/3GPP/Specs/25308-940.pdf>. Accessed 23 Sept 2011
9. USRP N200 series motherboards datasheet https://www.ettus.com/product/category/USRP_Networked_Series. Accessed 29 May 2012
10. USRP daughterboards datasheet <https://www.ettus.com/product/category/Daughterboards>. Accessed 29 May 2012
11. Universal Hardware Driver <http://ettus-apps.sourcerepo.com/redmine/ettus/projects/uhd/wiki>. Accessed 23 Sept 2011
12. AV Nikitin, RL Davidchack, Signal analysis through analog representation. *Proc R Soc Lond A.* **459**(2033), 1171–1192 (2003)
13. AV Nikitin, RL Davidchack, Adaptive approximation of feedback rank filters for continuous signals. *Signal Process.* **84**(4), 805–811 (2004)
14. AV Nikitin, RL Davidchack, Method and apparatus for analysis of variables, US Patents 7,133,568, 7 Nov 2006 and 7,242,808. (2007)
15. AV Nikitin, Method and apparatus for real-time signal conditioning, processing, analysis, quantification, comparison, and control, US Patents 7,107,306, 12 Sep 2006, 7,418,469, 26 Aug 2008, and 7,617,27. (2009)
16. C Berrou, A Glavieux, P Thitimajshima, Near Shannon limit error-correcting coding and decoding, in *Proc IEEE Int Conf Commun (ICC)*, Geneva, Switzerland, pp. 1064–1070 (1993)
17. 3rd Generation Partnership Project; Technical Specification Group Radio Access Network; Physical layer procedures (FDD) (Release 9) <http://www.quintillion.co.jp/3GPP/Specs/25214-910.pdf>. Accessed 23 Sept 2011
18. The Coded Modulation Library <http://www.iterativesolutions.com/Matlab.htm>. Accessed 23 Sept 2011
19. FTW OFDM Frame Encoder <https://www.cgran.org/wiki/ftw80211ofdmx>. Accessed 29 May 2011
20. FCC ID BCG-E2380B, 06 test report part 15C. <https://fjallfoss.fcc.gov/oetcf/eas/reports/ViewExhibitReport.cfm?mode=Exhibits&RequestTimeout=500>

&calledFromFrame=N&application_id=287555&fcc_id=BCG-E2380B' (2010). Accessed 23 Sept 2011

21. Abramowitz M, Stegun IA (eds.), *Handbook of Mathematical Functions with Formulas, Graphs, and Mathematical Tables*, 9th edn. (Dover, New York, 1972)
22. MS Han, J Choi, Multiband MIMO antenna with a band stop filter for high isolation characteristics, in *Antennas and Propagation Society International Symposium*, North Charleston, SC, pp. 1–4 (2009)
23. G Yue, W Shihua, F Oluyemi, C Xiadong, P Clive, C Laurie, Mutual coupling effects on pattern diversity antennas for MIMO femtocells. *Int J Antennas Propag* <http://www.hindawi.com/journals/ijap/2010/756848/>. Accessed 23 Sept 2011
24. Ettus Research LLC, DBSRX2. <http://code.ettus.com/redmine/ettus/attachments/88/dbsrx2.pdf>. Accessed 23 Sept 2011

doi:10.1186/1687-6180-2012-79

Cite this article as: Nikitin et al.: Impulsive interference in communication channels and its mitigation by SPART and other nonlinear filters. *EURASIP Journal on Advances in Signal Processing* 2012 **2012**:79.

Submit your manuscript to a SpringerOpen® journal and benefit from:

- Convenient online submission
- Rigorous peer review
- Immediate publication on acceptance
- Open access: articles freely available online
- High visibility within the field
- Retaining the copyright to your article

Submit your next manuscript at ► springeropen.com